**Thesis**

# Targeting bone sialoprotein (BSP) in an experimental model of uremic medial calcification


submitted by

**Patrick Christian Ganß, B.Sc.**


in partial fulfilment of the requirements for the degree of

**Doktor der gesamten Heilkunde**

**(Dr. med. univ.)**

at the

**Medical University of Graz**

executed at


**Medical University of Graz**

**Department of Internal Medicine**

**Division of Nephrology**

under the supervision of

**Univ. Prof.in Priv.-Doz.in Dr.in med.univ. Kathrin Eller**

**Dr.med.univ. Max Schuller**


Graz, 20.11.2023

*Declaration of Academic Integrity*

*I hereby confirm that the present diploma thesis is the result of my own independent scholarly work. I also confirm that in all cases, where material from the work of others (in books, articles, essays, dissertations, and on the internet) is acknowledged, quotations and paraphrases are clearly indicated. No material other than that cited in the reference list has been used. I have read and understood the Medical University's regulations and procedures concerning plagiarism.*

*Graz, 20.11.2023* *Patrick Ganß m.p.*

# Danksagungen

Ich bedanke mich recht herzlich bei der AG Eller und insbesondere bei Univ. Prof.in Priv.-Doz.in Dr.in med.univ. Kathrin Eller und Dr.med.univ. Max Schuller für die Möglichkeit, meine Diplomarbeit im Rahmen dieses spannenden Projektes anfertigen zu dürfen. Weiters möchte ich mich auch für die Unterstützung hinsichtlich Planung und Durchführung der Versuche und kurzfristige Anpassungen bedanken.

Mein Dank gilt insbesondere auch Corinna Schabhüttl, BSc. Danke für die Hilfestellungen, Tipps und Tricks. Mir hat die Zeit im Labor sehr viel Spaß gemacht.

Ich möchte mich natürlich auch bei meinen Eltern bedanken. Ohne sie wäre mein Studium nicht möglich.

# Zusammenfassung in Deutsch

**Einleitung:** Hohe Phosphatspiegel sind eine typische Folge der fortgeschrittenen chronischen Nierenerkrankung (CKD). Phosphat triggert die Transdifferenzierung der glatten Muskelzellen (VSMCs) der Tunica media der Gefäßwände zu einem osteoblastischen Phänotyp. Dabei wird die Expression von Kalzifizierungsinhibitoren herunter reguliert und gleichzeitig wird die Expression von Kalzifizierungspromotoren wie beispielsweise bone sialoprotein (BSP) und Kollagen Typ I gesteigert. Dies führt auch zu einer Änderung in der Zusammensetzung der extrazellulären Matrix innerhalb der Tunica media. BSP spielt bei der Entstehung von Hydroxylapatit-Kristallen eine Schlüsselrolle, da es als Nukleationskern für diese Kristalle dient, die dann in die Tunica media der Gefäßwand eingebaut werden. Dies führt schlussendlich zur Mediaverkalkung mit Komplikationen wie isolierter systolischer Hypertonie, einer verminderten Perfusion der Koronararterien und Schäden der Mikrogefäße insbesondere in den Nieren und im Zentralnervensystem.
In der gegenwärtigen Studie untersuchten wir die Applikation von anti-BSP-Antikörpern als potenzielle Therapieoption der urämischen Mediaverkalkung.

**Material und Methoden:** Fünf Gruppen mit je zehn weiblichen DBA2/N-Mäusen erhielten je vier intraperitoneale Injektionen der jeweiligen Antikörper bzw. des Vehikels über einen Zeitraum von 16 Tagen. Drei Gruppen wurde der monoklonale Antikörper FP21 in unterschiedlichen Dosierungen verabreicht (0,4 mg/mL; 1,2 mg/mL und 3,6 mg/mL). Die verbleibenden zwei Gruppen dienten als Kontrollgruppen. Von diesen erhielt eine Gruppe Phosphate-buffered saline (PBS) und die andere den Referenzantikörper IDK-1. Bei IDK-1 handelt es sich um einen rattenspezifischen monoklonalen anti-BSP-Antikörper, der in diesem Versuchsaufbau bei Mäusen keine Wirkung zeigen sollte. Am 8. Tag wurden alle Mäuse auf eine Hochphosphatdiät umgestellt. Diese enthielt 20,2 g Phosphor, 9,4 g Kalzium, 0,7 g Magnesium und 500 IU/kg Vitamin D3 je Kilogramm. Nach acht Tagen Hochphosphatdiät wurde der Kalziumgehalt der Nieren, Herzen und abdominellen Aorten, sowie die Konzentration des Serum-Harnstoffs bestimmt. Weiters erfolgte eine histologische Färbung der Herzen und Nieren mit Alizarin Red zur Darstellung von Kalziumablagerungen.

**Ergebnisse:** Sowohl in den histologischen Färbungen der Nieren und Herzen, als auch in der Bestimmung des Kalziumgehalts der Herzen, Nieren und abdominellen Aorten konnten keine signifikanten Unterschiede zwischen den Gruppen festgestellt werden. Dies gilt auch für die Serum-Harnstoff-Werte als Marker der Nierenfunktion.

**Diskussion:** Unsere Ergebnisse zeigten keinen Effekt des anti-BSP Antikörpers FP21 auf die untersuchten Parameter in unserem Hochphosphat-Modell. Weiters beschränkten sich unserer Untersuchungen auf „harte“ Outcome-Parameter und eine potentielle Änderung des VSMC-Phänotyps wurde nicht untersucht. Als entscheidende Limitation ist der hohe Schweregrad unseres Modells zu nennen, der eine längere Behandlungsdauer nicht zugelassen hat. Die Applikation von FP21 in einem adaptierten Tiermodell könnte weiterführend untersucht werden.

# Abstract in English

**Introduction:** High phosphate levels are a typical consequence of advanced stages of chronic kidney disease (CKD). Phosphate triggers the transdifferentiation of vascular smooth muscle cells (VSMCs) of the tunica media of vessel walls to an osteoblastic phenotype. This goes along with a down-regulation of calcification inhibitors and an increase in calcification promotors like bone sialoprotein (BSP) and collagen type I is increased, which leads to a change in the composition of the extracellular matrix within the tunica media. BSP has a key role in formation of hydroxyapatite crystals as it serves as nucleation site for these crystals, which are subsequently embedded in the tunica media of the vessel wall. This results in medial calcification with complications such as isolated systolic hypertension, decreased perfusion of coronary arteries and damage to the microvasculature, especially in kidneys and in the central nervous system.
In the present study, we investigated the application of anti-BSP-antibodies as potential therapeutic option for uremic medial calcification.

**Materials and Methods:** Five groups with ten female DBA2/N mice each received four intraperitoneal injections of the respective antibody of vehicle each over a period of 16 days. Three groups were treated with the monoclonal antibody FP21 in different concentrations (0.4 mg/mL, 1.2 mg/mL, 3.6 mg/mL). The remaining two groups served as control groups. One group was treated with phosphate-buffered saline (PBS) and the other one with the reference antibody IDK-1. IDK-1 is a rat monoclonal anti-BSP-antibody, which should not show any effect in mice. On day 8, diet was changed from standard chow to a high-phosphate diet. This diet contained 20.2 g of phosphorus, 9.4 g of calcium, 0.7 g of magnesium, and 500 IU/kg of vitamin D3 per kilogram. After eight days of high-phosphate diet, calcium content of kidneys, hearts and abdominal aortas was determined as well as concentration of blood urea nitrogen (BUN). Furthermore, histological staining of calcium deposits with Alizarin Red of heart and kidney samples was performed.

**Results:** Histological staining of kidney and heart samples, as well as the determination of calcium content of kidney, heart and abdominal aortas did not show significant differences between the groups. Similarly, BUN levels as a marker for kidney function were comparable between the groups.

**Discussion:** Our results did not show any effect of the anti-BSP antibody FP21 on the investigated outcomes in our high-phosphate model. Furthermore, our study focused on "hard" outcome parameters and potential alteration of VSMC phenotype was not examined. A major limitation was the severity of this model, which did not allow a longer duration of treatment. The application of FP21 in a modified animal model could be further investigated.

## Indication of publications already made

No publications have been made.

# Table of Contents

# Abbreviations

**#**

| | |
|---|---|
| °C | degree Celsius |
| λ | wavelength lambda |
| µ | micro |

**A**

| | |
|---|---|
| AA | abdominal aorta |
| *Abcc6* | ATP-binding cassette sub-family C member 6 |
| ACE | Angiotensin-converting enzyme |
| ANOVA | Analysis of variance |
| AP | Alkaline phosphatase |
| ARB | Angiotensin II receptor blockers |

**B**

| | |
|---|---|
| BCA | bicinchoninic acid assay |
| BMP2 | bone morphogenic protein-2 |
| BMP7 | bone morphogenic protein-7 |
| BSA | bovine serum albumin |
| BSP | bone sialoprotein |
| BW | body weight |

**C**

| | |
|---|---|
| C | heart/cor |
| c | concentration |
| Ca × P | calcium-phosphorus product |
| CD | cluster of differentiation |
| CD40L | cluster of differentiation 40 ligand |
| CKD | chronic kidney disease |
| CKD-MBD | chronic kidney disease-mineral bone disorder |

**D**

| | |
|---|---|
| Da | Dalton |
| DBA/2 | dilute-brown agouti 2 (mice) |

**E**

| | |
|---|---|
| ECM | extracellular matrix |
| eGFR | estimated glomerular filtration rate |
| ESC | European Society of Cardiology |
| ESKD | end-stage kidney disease |

**F**

| | |
|---|---|
| FGF23 | fibroblast growth factor 23 |

**G**

| | |
|---|---|
| g | grams |
| GFR | glomerular filtration rate |

**H**

| | |
|---|---|
| HCl | hydrochloric acid |
| HIF1α | Hypoxia-inducible factor 1α |
| ho-LDL | highly-oxidized-LDL |
| HPD | high phosphate diet |

**I**

| | |
|---|---|
| i.p. | intraperitoneal |
| IFNγ | Interferon gamma |
| IgM | Immunoglobulin M |
| IL-6 | Interleukin-6 |
| IQR | interquartile range |
| IU | international units |

**K**

| | |
|---|---|
| K | Kidney |
| k | kilo (prefix) |
| KDIGO | Kidney Disease: Improving Global Outcomes |

**L**

| | |
|---|---|
| L | litres |
| LDL | low density lipoprotein |

**M**

| | |
|---|---|
| m | milli (prefix) / metres |
| M | molar |
| MGP | matrix-gla-protein |
| min | minute |
| miRNA | microRNA / micro-ribonucleic acid |
| mmHg | millimetre of mercury |
| MMP-2 | matrix metalloproteinase-2 |
| mol | mole |
| mo-LDL | minimal-oxidized-LDL |
| MSX-2 | Msh homebox 2 |
| mTOR | mechanistic Target of Rapamycin |

**N**

| | |
|---|---|
| n | nano (prefix) |
| NaOH | sodium hydroxide |
| NF-κB | nuclear factor 'kappa-light-chain-enhancer' of activated B-cells |

**O**

| | |
|---|---|
| OD | optical density |

**P**

| | |
|---|---|
| PBS | phosphate buffered saline |
| PiT1 | type III sodium-dependent phosphate cotransporter |
| PTH | parathyroid hormone |

**Q**

| | |
|---|---|
| qPCR | quantitative polymerase chain reaction |

**R**

| | |
|---|---|
| RAAS | renin–angiotensin–aldosterone system |
| RGD | arginyl-glycyl-aspartic acid |
| ROS | reactive oxygen species |
| Rpm | rounds per minute |
| Runx2 | Runt-related transcription factor 2 = core-binding factor subunit alpha-1 |

**S**

| | |
|---|---|
| S | serum |
| SDS | sodium dodecyl sulphate |
| SGK1 | serum and glucocorticoid-regulated kinase 1 |
| SGLT2 | sodium-glucose transport protein 2 |
| SIBLING | small integrin-binding, N-linked glycoproteins |
| SM22α | smooth muscle protein 22 α |
| SMC | smooth muscle cell |
| *Sox9* | SRY-box transcription factor 9 |

**T**

| | |
|---|---|
| TA | thoracic aorta |
| TGF-β | transforming growth factor beta |
| TLR4 | toll-like receptor 4 |
| TNF-α | tumour necrosis factor alpha |

**V**

| | |
|---|---|
| VSMC | vascular smooth muscle cell |

# List of Figures

# List of Tables

# 1 Introduction

## 1.1 Chronic kidney disease

### 1.1.1 Chronic kidney disease in general

KDIGO-Guidelines define chronic kidney disease (CKD) "*as abnormalities of kidney structure or function, present for >3 months, with implications for health and CKD is classified based on cause, GFR category, and albuminuria category (CGA)*" (1). The glomerular filtration rate (GFR) is the blood volume filtrated by the glomeruli per minute normalized to the body surface in the dimension of mL/min/1.73 m² and is physiologically around 125 mL/min/1.73 m² in young adults and decreases with ageing by approximately 1 mL/min/year (1-3). There are different ways to determine the GFR e.g. via measurement of the clearance of freely filtered substances like inulin (which is the gold standard) or creatinine, but an estimated GFR (eGFR) is used more often for a first assessment of kidney function by determination of creatinine levels in plasma (2). The most common way to calculate the eGFR is the CKD-EPI formula which takes age and gender into account (4). But the creatinine blind range should be considered, as creatinine is actively excreted by the kidneys creatinine levels do not increase until the GFR and thus the kidney function is decreased by approximately 50 % (5).

CKD is the common consequence of different underlying diseases such as diabetic and/or vascular nephropathy, glomerulonephritis, interstitial nephropathy, chronic pyelonephritis, polycystic kidney disease or systemic diseases which all lead to damaged nephrons and consequently to a progressing and irreversible decrease of the GFR. The function of the kidneys include secretion of waste products, maintenance of acid-alkaline balance, volume and electrolyte homeostasis as well as regulation of blood pressure. In addition, the kidneys function as an endocrine organ as they synthesize renin, erythropoietin and hydroxylate and thus activate calcidiol to calcitriol (active form of vitamin D). The symptoms of CKD patients are due to decreased/lost kidney functions and therefore manifold: e.g. anaemia (and thus anaemic symptoms like paleness, tachycardia, fatigue), arterial hypertension, derailed electrolyte metabolism, metabolic acidosis and CKD mineral and bone disorder (CKD-MBD) (5, 6).

As mentioned above, CKD is classified by the GFR and albuminuria (measured as albumin/creatinine ratio in urine). The GFR-category (G) is divided into the stages G1-G5 according to the patient's GFR and the albuminuria category into A1-A3 according to the urinary albumin/creatinine ratio. The categories also allow for risk stratification (Figure 1) (1).

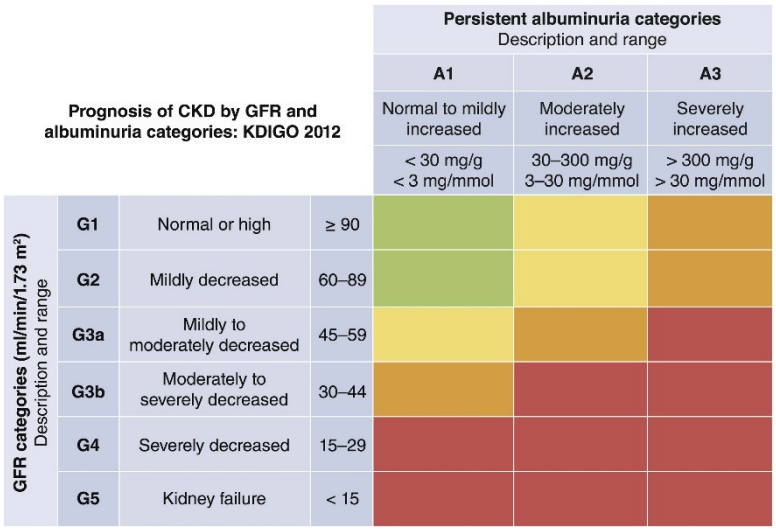


**Figure 1**: KDIGO CKD risk prognosis; Green, low risk (if no other markers of kidney disease, no CKD); yellow, moderately increased risk; orange, high risk; red, very high risk. (7)

"Uraemia" describes the accumulation of urinary substances in the blood due to impaired kidney excretion and can manifest by a range of symptoms, such as neural and muscular symptoms (e.g. fatigue, decreased mental acuity, seizures, sleep disturbances), endocrine and metabolic symptoms (e.g. amenorrhea, altered amino acid levels, CKD-MBD and others like serositis and platelet dysfunction) (8).

Therapy of CKD relies on several pillars. First, the underlying primary disease should be treated. Second, the progression of CKD should be stopped or slowed down by consequent treatment of hypertension with a target of ≤125/75 mmHg (although target levels differ between guidelines), protein restrictive diet (≤1 g/kg bodyweight daily) and in case of diabetes patients also consequent treatment of hyperglycaemia. Another pillar is the symptomatic therapy and mitigation of CKD-related complications. Hyperphosphatemia is treated with phosphate restricted diets or phosphate binders. A potassium restrictive diet and potassium binders are used to combat hyperkalaemia. Recombinant erythropoietin, iron substitution and, recently also, HIF1α stabilizing drugs are implemented in anaemia. Correction of pH with bicarbonate is often necessary due to metabolic acidosis. Volume overload or oedema demand salt restriction and loop diuretics. However, caution is

warranted when using potassium sparing diuretics like spironolactone, as CKD patients are at an increased risk of hyperkalaemia (5, 9-11).

Antihypertensive therapy with inhibition of the renin–angiotensin–aldosterone system (RAAS) by angiotensin-converting enzyme (ACE) inhibitors or angiotensin II receptor blockers (ARBs) has a nephroprotective effect (12, 13). Studies like the CREDENCE and DAPA-CKD study underline also a nephroprotective effect of gliflozins, which are inhibitors of sodium-glucose transport protein 2 (SGLT2), even in patients with CKD of non-diabetic genesis (14-16).

If conservative therapy is not sufficient and the patient still suffers from hyperhydration with fluid lung, hyperkaliaemia, metabolic acidosis, uremic pericarditis or gastritis, kidney replacement therapy is indicated (absolute indications). Kidney replacement therapies can be separated into extracorporeal blood purification methods (i.e. haemodialysis, hemofiltration and hemodiafiltration as a combination of the two aforementioned), peritoneal dialysis and kidney transplantation (5).

## 1.2 Arteriosclerosis

The term “arteriosclerosis” characterizes the hardening and increasing stiffness of arterial walls in general and can be differentiated into atherosclerosis, medial calcification and arteriolosclerosis (17). This differentiation depends on histological criteria on the one hand and vessel size on the other.

The wall of arteries consists of three different layers: The tunica adventitia is the outermost layer which is formed by connective tissue and contains fibroblasts, proteoglycans, elastic and collagen fibres and the vasa vasorum. The middle layer – called tunica media – is the thickest layer and is formed by vascular smooth muscle cells (VSMC) and extracellular matrix (ECM), which again is formed by the VSMCs. The third and innermost layer is the tunica intima and consists of endothelium and a subendothelial layer. These three layers are separated by two elastic lamellae: The external elastic lamina forms the border between tunica adventitia and tunica media and the internal elastic lamina between tunica media and tunica interna. The described structured layers are shown in Figure 2 (18).

Arteries can be distinguished into two different subtypes, namely muscular arteries and elastic arteries. While most arteries belong to the first subtype (including the small arteriolas with only one or two layers of VSMCs), those near the heart (i.e. aorta, pulmonary trunk and their respective major branches) are elastic arteries. Their medial layer contains many elastic

fibres and can therefore generate and maintain the so-called Windkessel effect to generate a constant blood flow (18, 19).

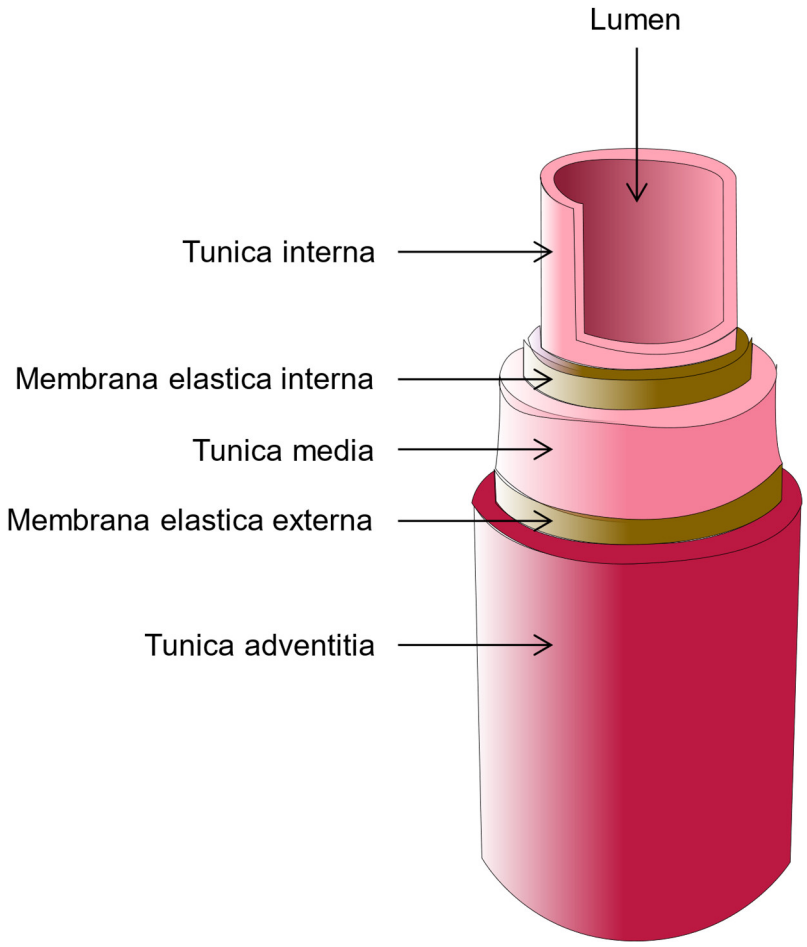


**Figure 2:** Schematic wall layer structure of a muscular artery (adapted from (20))

### 1.2.1 Atherosclerosis

Atherosclerosis is the modification of the tunica intima initiated by the deposition of atheromatous plaques (consisting of fatty deposits), which leads to a decreased blood flow and ultimately results in vascular diseases such as ischemic heart disease (>95 % caused by atherosclerosis), stroke (70 % caused by atherosclerosis) and peripheral arterial disease (90 % caused by atherosclerosis) (5, 17, 21). Cardiovascular disease as a consequence of atherosclerosis poses a major risk factor for premature mortality and disability-adjusted life years (22). The pathogenesis of atherosclerosis is complex and can be divided into different phases (17):

1. Initial phase: Risk factors such as arterial hypertension, tobacco consumption, toxins, hemodynamic stress and hyperlipidaemia causes endothelial dysfunction of the tunica intima. This leads to an increased permeability of the endothelium

with subsequent influx of lipoproteins. Low-Density-Lipoprotein (LDL) can be oxidized in the intimal tissue (17).

2. Inflammatory phase: Increased chemokine production, triggered by the resulting minimal-oxidized-LDL (mo-LDL), leads to adhesion and immigration of neutrophilic granulocytes and monocytes, which differentiate into macrophages (17).
3. Formation of foam cells and fatty streaks: LDL is highly oxidized by reactive oxygen species (ROS) and other enzymes. This resulting highly-oxidized-LDL (ho-LDL) is taken up by the immigrated macrophages via their Scavenger-receptors resulting in the formation of lipid-laden macrophages – also called foam cells. Multiple layers of these foams cells and lipid droplets (as a result of destroyed macrophages) assemble to form the visible fatty streaks (17).
4. Formation of fibrous plaques: Immigration of T-lymphocytes is the result of inflammatory reactions caused by macrophages. The interaction of CD40 (Cluster of Differentiation) and its ligand CD40L stimulates a release of cytokines – such as Interferon-γ (IFNγ) – from T-lymphocytes and macrophages. This ongoing inflammatory reaction leads to immigration and proliferation of VSMCs and thus to the formation of a fibrous plaque (17).
5. Formation of complex lesions and thrombosis: An instable matrix is caused by IFNγ, as it inhibits the production of extracellular matrix and instability is enhanced by various proteases such a collagenases, gelatinases and stromolysin, resulting in an increased risk of ulceration. The calcification of the lesion is an active and self-regulated process as microvascular pericytes and VSMCs can generate mineralized matrix and differentiate into osteoblastic-like cells (23). Rupture of the plaques leads to thrombus formation with exposition of tissue-factor and a necrotic atheromatous nucleus. These thrombi can occlude vessels partially or completely (17).

Ruptured atherosclerotic plaques are the most common cause of acute thrombosis in coronary arteries leading to myocardial infarction (24). Apart from ischemic heart disease, stroke and peripheral arterial disease, atherosclerosis may also affect renal arteries leading to reduced kidney function and renal hypertension (24).

Due to the multifactorial pathogenesis of atherosclerosis, prevention focuses on the underlying risk factors. Lifestyle changes, which do not involve any pharmaceuticals, have positive effects on several risk factors, and are thus the bedrock of therapy (24).

The 2021 ESC Guidelines on cardiovascular disease prevention in clinical practice recommend lifestyle changes including regular physical activity, a Mediterranean diet and smoking cessation for all individuals. Hyperlipidaemia and hypertension are important risk factors for atherosclerotic diseases, and lifestyle modification has positive effects on those risk factors as well. However, pharmacological antihypertensive and/or lipid-lowering therapy is recommended in all risk patients (25).

Therefore all CKD patients with an age of 50 years or older should receive a statin treatment and in those CKD patients with a GFR category of G3a or above, dual therapy with a combination of a statin and ezetimibe should be considered (26).

### 1.2.2 Arteriolosclerosis

Arteriolosclerosis is the hyalinisation of the wall of arteriola. Initially affecting the tunica intima, but also extending to the whole wall with further progression, this process leads to constriction of the vessels. Some authors differentiate two histological forms of arteriolosclerosis: hyaline arteriolosclerosis is described as the intimal hyalinisation and can be found in kidneys of patients with diabetes mellitus, patients with systemic arterial hypertension and physiologically in aging patients, whereas medial hyperplasia and hypertrophy leads to hyperplastic arteriolosclerosis and is caused by malignant hypertension (17, 27-29).

The pathogenesis of the (hyaline) arteriolosclerosis is not yet fully understood. However it is suspected, that dysfunctional endothelium and overproduction of hyaline eosinophilic material including proteoglycans, lipids, immunoglobulin M (IgM), complement factors and fibrinogen by endothelial cells results in vascular constriction (17). In the kidneys, stenosis of arteriola leads to chronic ischemia and atrophy of the affected nephrons (17).

### 1.2.3 Medial calcification

Medial calcification describes an accumulation of calcium phosphate crystals in the tunica media of the arterial wall which consequently leads to increased arterial stiffness. In contrast to atherosclerosis, medial calcification is a non-occlusive condition (30-32).

Medial calcification in extremity arteries was firstly described as a distinct entity from atherosclerosis by Johann Georg Mönckeberg in 1903 and is the most common type of medial arterial calcification (33, 34). Medial calcification is strongly associated with diabetes mellitus and chronic kidney disease (CKD) (35). According to Lanzer et al., the prevalence of medial calcification is unknown, because it is often an incidental finding or misdiagnosed as atherosclerosis (31). Hoek et al. reported in a cross-sectional study, that in 718 participants with cardiovascular disease – or the risk to develop such – 25 % displayed signs of medial arterial calcification in computed tomography scans (36). Yet, the ankle-brachial index (which was thought to be valid diagnostic method) was only elevated (> 1.4) in 8.7 % of the participants (31, 33, 36).

Kamenskiy et al. examined femoropopliteal arteries of 431 tissue donors (mean age 53±16 years) histologically and diagnosed medial arterial calcification in 46 % of the examined arteries (37). These findings underline the lack of a sensitive screening method for medial calcification.

Although medial calcification is a distinct entity, it can occur together with atherosclerosis and is also associated with hyperparathyroidism, ageing, vitamin-D-disorders and others (33).

Stiffening of large arteries (such as aorta) induces systolic hypertension, decreased coronary perfusion and increased afterload of the left ventricle of the heart (38-40). Increased pulsatile stress damages the microvasculature of brain and kidney (41, 42).

Furthermore medial arterial calcification also propagates peripheral arterial disease (43).

### 1.2.3.1 Characterization of vascular smooth muscle cells (VSMCs)

VSMCs play a major role in medial calcification. VSMCs can derive from different embryonic origins, i.e. neural crest, secondary heart field, somites, mesoangioblasts, proepicardium, splanchnic mesoderm and mesothelium (44). For example, VSMCs which are relevant for septation of aorta and pulmonary trunk derive form the cranial neural crest, whereas the smooth muscle cells of the coronary system do not derive from neural crest but from proepicardium (44-46). A unique characteristic of these cells is, that they are – unlike other muscle cells – not terminally differentiated, but can alter their phenotype depending on the environment or environmental changes respectively (47, 48). VSMCs in mature blood vessels are characterized by a very low proliferation rate and synthetic activity as well as specific expression pattern (see chapter 1.2.3.2) (49). Upon damage of the vessel's wall, however, synthetic and proliferative activity is increased leading to a synthetic phenotype which is essential to restore the integrity of the affected wall (49). Furthermore, the embryonic origin of VSMCs may determine their susceptibility for calcification (50). Kirsch et al. showed, that calcification takes place mainly in the abdominal aorta (which has VSMCs with mesenchymal origin), but not in the aortic arch nor in the ascending thoracic aorta, where VSMCs derive from neural crest (44, 50, 51).

### 1.2.3.2 Molecular mechanism of medial calcification

#### 1.2.3.2.1 Transdifferentiation

Medial calcification is an actively regulated process sharing elements with bone formation and includes formation of hydroxyapatite (32, 33). Physiologically, mature VSMCs in arterial walls have a quiescent-contractile phenotype that corresponds to regulation of vascular tone as their primary role and accordingly express smooth muscle specific markers like for example smooth muscle myosin heavy chain, smooth muscle α-actin and smooth muscle protein 22 α (SM22α) (48, 52, 53).

However, VSMCs are able to change their phenotype. This is marked by upregulation of osteogenic and chondrogenic transcription factors such as Runt-related transcription factor 2 (Runx2), Msh homebox 2 (MSX-2), bone morphogenic protein-2 (BMP2), SRY-box transcription factor 9 (*Sox9*) and osterix. This transdifferentiation of VSCMs into an osteoblastic phenotype is followed by the expression of bone sialoprotein (BSP), alkaline

phosphatase (AP), osteocalcin and collagen type I. These proteins have been detected in calcified arteries. (54-56)

The transdifferentiation to an osteoblastic phenotype is also characterized by a loss of smooth muscle specific markers like SM22α and smooth muscle α-actin (57).

#### 1.2.3.2.2 Activators and inhibitors of calcification

To prevent spontaneous mineralization, calcification inhibitors like pyrophosphate, matrix-gla-protein (MGP), α-2-Heremans-Schmid-Glycoprotein (fetuin-A), bone morphogenic protein-7 (BMP7), osteopontin and osteoprotegerin are produced or taken up by VSMCs (56, 58, 59).

Another factor contributing to calcification is the loss of these inhibitors as a result of upregulated osteogenic transcription factors or in specific genetic conditions (58). For example, loss or reduced MPG, due to high calcium levels or in Keutel-syndrome, leads to BMP2 overexpression and intensified medial calcification (58, 60, 61). As MPG depends on vitamin-K as a cofactor, vitamin-K deficiency (e.g. warfarin as anticoagulant therapy) leads to a similar phenotype (62). Fetuin-A can bind to BMP2 as well as transforming growth factor beta (TGF-β) and acts as a protector from vascular calcification (63, 64). In patients with pseudoxanthoma elasticum, a genetic syndrome with a *Abcc6*-loss characterized by progressive mineralization of elastic fibres, reduced MGP and fetuin-A levels are found (65, 66).

Pyrophosphate – a potent inhibitor of calcification – blocks hydroxyapatite crystal formation, but is cleaved by alkaline phosphatase (AP), which is upregulated by osteoblastic VSMCs (67, 68).

Elevated AP levels are also detectable in CD73-deficient patients. CD73 converts adenosine-monophosphate to adenosine. In case of CD73 deficiency, adenosine levels decrease, which leads to a compensatory increase of tissue-nonspecific AP. Tissue-nonspecific AP is also capable of generating adenosine by hydrolyzation of adenosine monophosphate to adenosine. Hence, due to increased AP-mediated pyrophosphate cleavage, CD73-deficient patients are at an increased risk of calcification (69-71).

PHOSPHO1 is another phosphatase with an impact on bone formation and vascular calcification. Matrix vesicles, which act as nucleation sites for bone and ectopic calcification contain this enzyme. Suppression of PHOSPHO1 prevents calcification of VSMCs (72, 73).

Furthermore, aging is associated with calcification. Decreased MGP expression, increased AP and upregulated Runx2 can be detected in senescent VSCMs, possibly due to prelamin-A accumulation (58, 74).

Klotho, an inhibitor of calcification, has been shown to be progressively lost with aging. Hu et al. showed, that loss of Klotho leads to an upregulation of type III sodium-dependent phosphate cotransporter PiT1 and Runx2, decreased SM22, and ultimately promotes calcification (75, 76).

Other factors contributing to enhanced Runx2 expression are oxidative stress and mitochondrial dysfunction (58, 77).

Quiescent-contractile VSMCs express calcium-sensing receptors, which inhibit the transition to an osteoblastic mineralizing phenotype. High extracellular levels of calcium decreases the expression of calcium-sensing receptors and thus promotes the osteoblastic phenotype of VSMCs, but the exact mechanism is still unknown (58, 78).

The role of vitamin D in medial calcification is ambiguous. On the one hand, vitamin D was proven to induce medial calcification via Runx2, but can be blocked by BMP7 (59, 79). On the other hand, vitamin D leads to upregulation of calcium-sensing receptors on the surface of VSMCs *in vitro* via activation of vitamin D receptor and thus inhibits calcification (80).

Furthermore, Bas et al. reported, that medial calcification induced by calcitriol in rats is partly reversed by monocytes/macrophages in otherwise healthy animals after cessation of calcitriol administration (81).

In summary, vascular calcification is linked with both, increased and decreased levels of vitamin D, and the effect may potentially be dose-dependent (80, 82).

Finally, micro-RNAs (miRNAs) may also contribute to vascular calcification and their role has been reviewed extensively by Leopold (83).

#### 1.2.3.2.3 Role of phosphate

High phosphate levels can lead to a phenotypic change of VSMCs from quiescent-contractile to osteoblastic involving a multitude of signalling pathways. First, high phosphate leads to activation of type III sodium-dependent phosphate cotransporter PiT1, which is necessary for the upregulation of Runx2. Second, high phosphate (and high calcium) lead to an increased expression of BMP2 and a decreased expression of BMP7 (55, 84).

Furthermore, BMP2 increases expression of PiT1 (85). Increased expression of proteins like BSP and collagen type I lead to a transformed extracellular matrix (ECM) and contributes to calcification (56).

Intriguingly, Zhou et al. provided evidence for a kidney-bone axis implicated in phosphate homeostasis, where phosphate stimulates glycolysis in proximal tubules and glycolysis products promote bone fibroblast growth factor 23 (FGF23) production. If such an indirect phosphate-sensing pathway exists in the vasculature as well is currently unknown (86).

The transdifferentiation is also mediated via nuclear factor 'kappa-light-chain-enhancer' of activated B-cells (NF-κB). Toll-like receptor 4 (TLR4) signalling has been put forth as potential “phosphate sensor”. High levels of phosphate also lead to upregulation of serum and glucocorticoid-regulated kinase 1 (SGK1). TLR4 and SGK1 enhance NF-κB-signalling. NF-κB-signalling results in upregulation of the osteogenic transcription factors MSX-2 and Runx2 (87-91).

Apart from this NF-κB-signalling, calcification is also mediated via the Wnt/β-catenin pathway. High phosphate levels activate this pathway and lead therefore to upregulation of Runx2 and Pit1. The Wnt/β-catenin pathway and MSX-2 have been shown to activate each other, potentially creating a positive feedback loop (92-95).

Inflammation is another driver of calcification. Hyperphosphatemia promotes inflammation in aorta, kidney and heart, as evident by expression of inflammatory cytokines like tumour necrosis factor alpha (TNF-α) in VSMCs under hight-phosphate conditions. TNF-α in turn is another activator of the NF-κB-pathway (89, 96).

However, treatment with TNF-α inhibitor etanercept has not resulted in reduced aortic calcification in a mouse model of uremic media calcification (50).

Other proinflammatory cytokines expressed by VSMCs are Interleukin-6 (IL-6) and transforming growth factor beta (TGF-β). IL-6 leads to upregulation of BMP2. TGF-β leads via its signalling cascade ultimately to Runx2 upregulation (97-102).

Finally, hyperphosphatemia also leads to intracellular and mitochondrial ROS-formation in VSMCs, which then again enhances NF-κB-signalling (103).

#### 1.2.3.2.4 Mechanisms of hydroxyapatite formation

VSMCs release vesicles which do not calcify as they contain calcification inhibitors. However, with increasing extracellular calcium, matrix vesicles containing preformed apatite and fewer calcification inhibitors are secreted. These may act as nucleation site for ectopic calcification (61, 104).

Apart from matrix vesicles, apoptotic bodies released by dying VSMCs due to high levels of calcium, serve as nucleation sites as well (105, 106).

Similarly, bone sialoprotein (BSP) also induces formation of hydroxyapatite (107).

### 1.2.3.3 Medial calcification in CKD-patients

According to Mills et al., the prevalence of CKD is approximately 10 % in men and around 12 % in women worldwide (108). Medial calcification can be found at any CKD-stage (109). A strict regulatory circuit controls the phosphate balance physiologically, but is deranged in patients with CKD (110). Patients with progressive CKD display deranged homeostasis of calcium, phosphorous, parathyroid hormone (PTH) and vitamin D, as well as impairment of bone metabolism leading to fractures and extra-skeletal calcification including arteries (111). This symptom complex is subsumed under the term Chronic Kidney Disease Mineral Bone Disorder (CKD-MBD) (111).

Initially, hyperphosphatemia due to nephron loss in CKD is compensated by increased phosphate excretion mediated by the phosphaturic hormones PTH and FGF23. However, with further decline of kidney function, these countermeasures fail and hyperphosphatemia ensues. Hyperphosphatemia inhibits synthesis of calcitriol (via FGF23) and thus leads to hypocalcaemia and increasing PTH levels, known as secondary hyperparathyroidism (111).

Therapeutic options include vitamin D agonists and calcium-containing phosphate binders, which both have hypercalcaemia as a side-effect (112). As mentioned above (see 1.2.3.2), both, hyperphosphatemia and hypercalcaemia may potentially aggravate vascular calcification. In addition, CKD patients show lower levels of pyrophosphate, which is further depleted due to haemodialysis (113). Moreover, Klotho expression is decreased in CKD patients and Klotho declines with progression of CKD (75, 114). FGF23 is paramount in maintaining phosphate and calcium homeostasis, but without the coreceptor Klotho, FGF23 cannot bind to its receptor, which downstream contributes to CKD-MBD (115, 116).

Plasma aldosterone levels are elevated in CKD patients, and aldosterone upregulates PiT1-cotransporter as well as Runx2 and MSX-2 by aldosterone dependent upregulation of SGK1, which in turn enhances NF-κB-signalling (91, 117, 118).
Independently of phosphate, uremic serum can increase Runx2 expression in VSMCs, a hallmark of osteoblastic transdifferentiation (8, 119).
In patients with chronic kidney failure, Interleukin-18 (IL-18) levels are elevated, which favours the osteogenic phenotype switch in VSMCs – partly by upregulation of SGK1 (120-122).
In summary, uraemia tips the balance towards pro-calcifying factors, via a plethora of different pathways, resulting in media calcification and its deleterious sequelae.

#### 1.2.3.4 Experimental Models of medial calcification

There are different well-established *in vivo* models for medial calcification, which are outlined in the following (123).
Medial calcification is developed by Han:SPRD Cy/+ rats and Lewis polycystic kidney disease rats naturally, due to kidney failure (124, 125). Kidney failure can also be induced surgically, usually by electrocoagulation or partial nephrectomy (126, 127). Furthermore, it can be obtained or mimicked by administrating special diets, like e.g. adenine or phosphate rich diets (128-130).
Genetically modified knock-out animals can also be used as model organisms. Due to lacks of substances required for physiological electrolyte homeostasis and/or calcification inhibitors, these animals (mostly mice) develop medial calcification. Among these are for example MGP knock-out mice, as well as fetuin-a-, *Abcc6*-, FGF23-knockout and Klotho-hypomorphic mice (66, 76, 131-133).
Many of the mice used as models are C57BL/6 mice regarding their genetic background, but these mice seem to be resistant to ectopic calcification (134, 135).

#### 1.2.3.4.1 DBA2/N mouse model

Another calcification model are dilute-brown agouti 2 mice (DBA/2). These mice and especially female DBA/2 mice tend to develop ectopic calcification (135-137). DBA/2 mice have an alternative splice variant in the gene *Abcc6* (137, 138). *Abcc6* is involved in the regulation of mineralization and dysfunctional or missing *Abcc6* leads to vascular calcification (66, 139).

This is partly explained by the impact of *Abcc6* on the pyrophosphate metabolism, as *Abcc6* increases extracellular pyrophosphate concentrations (139). Hence, a lack of *Abcc6* results in decreased concentration of the calcification inhibitor pyrophosphate (139).

Additionally, missing *Abcc6* leads to calcification via persistent expression of *Sox9* in aged mice (66).

This calcification tendency can be enhanced by increased oral phosphate intake (130).

Female DBA/2 mice are a well established model for ectopic and medial calcification (50, 136, 140).

## 1.3 Bone sialoprotein (BSP)

BSP can act as a nucleation site for hydroxyapatite (107). BSP is a major non-collagenous matrix protein of bone, and, together with osteopontin, dentin matrix protein I, dentin sialophosphoprotein and matrix extracellular phosphoglycoprotein, forms the family of small integrin-binding, N-linked glycoproteins (SIBLING) (141, 142). Human BSP is an acidic protein and has 301 amino acids with an average mass of approximately 50 kDa, but due to the fact that BSP is extensively posttranslationally modified, its molecular weight varies to a high degree (143, 144). Structural clarification of BSP was delivered by Vincent and Durrant (145).

According to Goldberg et al. the capability of BSP to act as hydroxyapatite nucleation site is due to its helically arranged glutamic acid-rich sequences (146). Furthermore, BSP features an arginyl-glycyl-aspartic acid sequence (RGD-motif), which is an integrin recognition site and mediates cell adhesion (147, 148). A molecular model of human BSP is depicted in Figure 3.

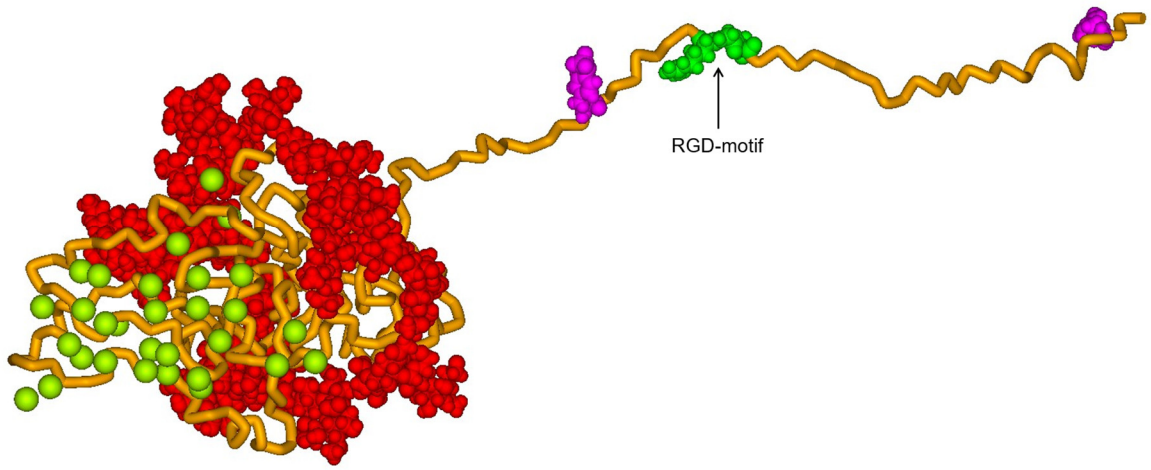


**Figure 3**: Molecular model of human BSP (modified illustration based on Marcus Durrant (149))

The main role of BSP is *de novo* formation of bone (150). Additionally, BSP is also implicated in cancer prognosis, as BSP is expressed in breast cancer and associated with higher probability of bone metastasis and poor outcome (151, 152).

Similar associations were found between BSP and other osteotropic cancers such as prostate cancer, thyroid cancer and multiple myeloma (153-155).

This effect of BSP might be due its RGD-motif, by which it binds the integrin $\alpha_V\beta_3$ and matrix metalloproteinase-2 (MMP-2), which is able to degrade the ECM. Thus, this triple complex can enhance invasiveness of cancer cells (156).

Zepp et al. showed that administration of IDK-1, a rat monoclonal antibody against BSP, in a rat model of induced metastatic skeletal lesions (via the human breast cancer cell line MDA-MB-231) leads to a dose-dependent regression of metastatic bone lesions (157). Furthermore, elevated BSP levels can be found in osteoblastic VSMCs as part of their typical expression pattern e.g. in calcified arteries (as described earlier). This leads to the hypothesis that BSP plays also an important role in ectopic and vascular calcification.

## 1.4 Hypothesis/Aim

As potential nucleation site for hydroxyapatite, BSP is critically involved in ectopic and vascular calcifications. We aimed to prevent calcification by blocking BSP using the mouse monoclonal antibody FP21 in DBA/2 mice on a high phosphate diet.

# 2 Materials and Methods

## 2.1 Approval

The animal experiments were performed under approval number BMBWF-60.010/0189-V/3b/2018 of the Federal Ministry of Education, Science and Research of the Republic of Austria.

## 2.2 The DBA/2-mouse model

Fifty female DBA2/NCrl (short DBA/2) mice were obtained from Charles River Laboratories (Sulzfeld, Germany) and housed in the laboratory animal facility of the Medical University of Graz in a virus-free environment. Mice were acclimatized for at least one week and randomized into five different groups as soon as they reached a mean weight of approximately 19-20 grams or above:

- group 1: vehicle-group (PBS), (n=10)
- group 2: reference antibody (rat monoclonal antibody IDK-1) (c = 3,6 mg/mL), (n=10)
- group 3: low-dose mouse monoclonal antibody FP21 (c = 0,4 mg/mL), (n=10)
- group 4: medium-dose mouse monoclonal antibody FP21 (c = 1,2 mg/mL), (n=10)
- group 5: high-dose mouse monoclonal antibody FP21 (c = 3,6 mg/mL), (n=10)

For logistic reasons, experiments were carried out in four different runs:
Run 1 and 2: three mice per group (in total 15 mice per run) and run 3a and 3b: two mice per group (in total 10 mice per run).
IDK-1 and FP21 antibody stock-solutions were obtained from Immundiagnostik AG (Bensheim, Germany) and diluted with sterile phosphate buffered saline (PBS) (Sigma Aldrich, St. Louis, USA) to the respective concentration freshly before each injection. Mice were fed with standard chow diet (ssniff-Spezialdiäten GmbH, Soest, Germany) until the diet was switched to high-phosphate diet (HPD) obtained by Altromin Spezialfutter GmbH & Co. KG (Lage, Germany). Standard chow diet contains 7.0 g of phosphorus, 10.0 g of calcium, 2.2 g of magnesium and 1000 IU/kg of vitamin D3 per kilogram. HPD contains 20.2 g of phosphorus, 9.4 g of calcium, 0.7 g of magnesium and 500 IU/kg of vitamin D3 per kilogram.
Intraperitoneal (i.p.) injections with a weight adjusted volume of 5 mL/kg bodyweight were started at day d-7, and after that every four days (i.e. d-3, d+1, d+5). On day d0, the diet was changed to HPD. At d+8 the mice were anesthetized and serum (S) was collected via

retrobulbar bleeding. Mice were perfused with 10 mL of sterile, ice-cold PBS, and then sacrificed by cervical dislocation. For further analysis, kidneys (K), hearts (C), and the thoracic and abdominal aortas (TA/AA) were collected. AA were dissected starting from the diaphragm until before the branching of the common iliac arteries. TA were dissected starting from the end of the aortic arch until the diaphragm. Remaining periaortic connective tissue was removed carefully using microsurgical instruments in ice-cold PBS. As they are particularly prone to calcification and TA appear somewhat protected, only AA were used for further investigation (50).

The timeline of the experiments is represented graphically in Figure 4.

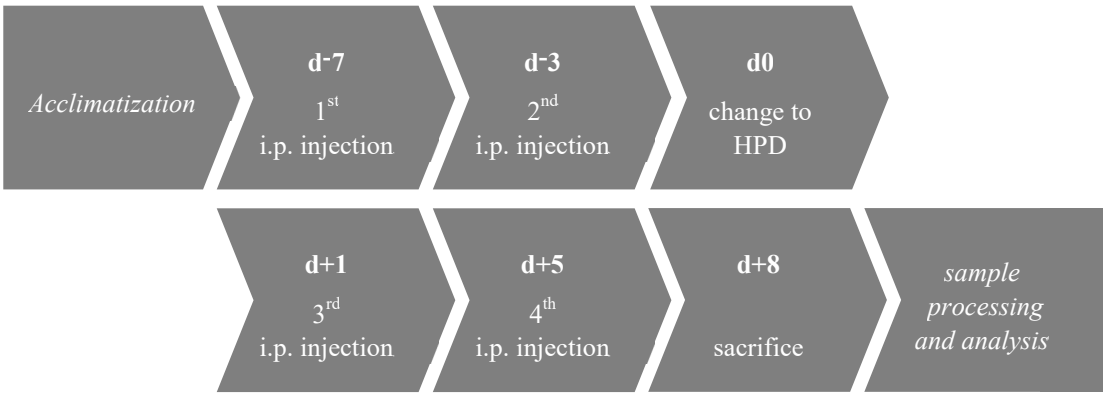


**Figure 4**: Timeline of Experiments

## 2.3 Determination of calcium concentration in aorta, kidney and heart

For decalcification, tissue slices of approximately 10-20 mg of heart's apices (C) and kidneys (K) respectively were added to 100 µL 0.6 M hydrochloric acid (HCl) (Merck KGaA, Darmstadt, Germany). The abdominal aortas (AA) were put into 70 µL 0.6 M HCl each. All probes were incubated at 37 °C and 100 rpm in an incubator shaker overnight. The following day, supernatants were taken off and centrifuged for 5 minutes at 10.000 rpm at room temperature. Supernatants were then used for calcium quantification. The remaining tissues were washed with 500 µL PBS (Sigma Aldrich, St. Louis, USA). Afterwards, heart and kidney tissues were lysed in a 100 µL mixture of 0.1 M sodium hydroxide (NaOH) (Merck KGaA, Darmstadt, Germany) and 0.1 % sodium dodecyl sulphate (SDS) (Sigma Aldrich, St. Louis, USA) (0.1 M NaOH/0.1 % SDS). The remaining aortic tissues were lysed in 70 µL 0.1 M NaOH/0.1 % SDS. All tissues were subsequently homogenised manually using a pestle. After 30 minutes of incubation at room temperature, all probes were

centrifuged for 5 minutes at 10,000 rpm at room temperature. Thereafter, supernatants were used for protein quantification.
The resulting calcium levels were then normalized to the protein content of the respective tissue probe as well as to the respective tissue wet weight. Recognizing their individual advantages and limitations, we decided to report results with both normalization methods.

### 2.3.1 Protein quantification

Protein levels of homogenised tissues were quantified using bicinchoninic acid assay (BCA) in a 96-well-microplate (Microplate, 96 well, PS, F-bottom, clear; Greiner Bio-One GmbH, Kremsmünster, Austria). This was done by employing the Pierce™ BCA Protein Assay Kit (Thermo Fisher Scientific Inc., Waltham, USA) and following the manufacture's instructions. Briefly, nine standards of bovine serum albumin (BSA) with concentrations of 2,000 µg/mL, 1,500 µg/mL, 1,000 µg/mL, 750 µg/mL, 500 µg/mL, 250 µg/mL, 125 µg/mL, 25 µg/mL and 0 µg/mL (diluted with 0.1 M NaOH/0.1 % SDS) were made. The probes of kidneys and hearts were diluted 1:20 with 0.1 M NaOH/0.1 % SDS and the probes of the abdominal aorta 1:5, respectively. 10 µL of each standard and sample were mixed with 200 µL of the manufacturer's working reagent and incubated for 30 minutes at 37 °C. All samples and standards were measured as duplicates. After the incubation, optical density (OD) measurements were carried out at a wavelength of $\lambda = 562$ nm using a FLUOstar omega photometer (BMG Labtech GmbH, Ortenberg (Baden), Germany) and the accompanying software.

### 2.3.2 Calcium quantification

Calcium quantifications were carried out with a QuantiChrom™ Calcium Assay Kit (DICA-500) (BioAssay Systems, Hayward, USA) according to the manufacture's instructions using a Greiner 96-well-microplate. Briefly, eight standards with calcium concentrations of 20 mg/dL, 16 mg/dL, 12 mg/dL, 8 mg/dL, 6 mg/dL, 4 mg/dL, 2 mg/dL and 0 mg/dL were made (diluted with distilled water). 5 µL pf each standard and sample were mixed with 200 µL of the manufacture's working solution and incubated for 3 minutes at room temperature. If necessary, samples were diluted with distilled water. All samples and standards were measured as duplicates. After the incubation, OD measurements were carried out at a wavelength of $\lambda = 612$ nm using a FLUOstar omega photometer (BMG Labtech GmbH, Ortenberg (Baden), Germany) and the accompanying software.

## 2.4 Histological quantification of kidney and heart calcification

Extracted kidneys (K) and hearts' bases (C) were fixed in 4 % paraformaldehyde and embedded in paraffin. Tissue slices of 4 µm were made using a microtome and mounted onto microscope slides. Two or three tissue samples were made per sample. These slides were then dried at 37 °C overnight.

### 2.4.1 Alizarin Red S Staining

For visualization of calcium deposits, these slides were stained with 2 % Alizarin Red S solution (pH 4.1-4.3) (Sigma Aldrich, St. Louis, USA). Firstly, the slides were deparaffinized in xylene and in a descending ethanol series (100 %, 90 %, 70 %) (Merck KGaA, Darmstadt, Germany) and distilled water. The slides were then stained in Alizarin Red S (Sigma Aldrich, St. Louis, USA) staining solution for two minutes and subsequently dehydrated in acetone (Merck KGaA), acetone-xylene-mixture (50:50) and xylene (Carl Roth GmbH + Co. KG, Karlsruhe, Germany). The slides were then enclosed after drying at room temperature.

### 2.4.2 Digital quantification

The coloured slides were digitalized and the resulting pictures cropped with QuPath 0.4.1 (Queen's University, Belfast, United Kingdom) (158). Afterwards, the ratio of stained calcium deposits over the whole tissue area (in % of whole tissue) was determined using ImageJ (NIH, Maryland, USA).

## 2.5 Blood urea nitrogen/BUN

To determine the kidney function, blood urea nitrogen of the collected sera was determined with Invitrogen™ Urea Nitrogen (BUN) Colorimetric Detection Kit (Thermo Fisher Scientific Inc., Waltham, USA) in a Greiner 96-well-microplate and according to the manufacture's instructions. Eight standards with urea nitrogen concentrations of 10 mg/dL, 5 mg/dL, 2.5 mg/dL, 1.25 mg/dL, 0.625 mg/dL, 0.3125 mg/dL, 0.156 mg/dL and 0 mg/dL were made (diluted with distilled water). All samples were diluted with distilled water in a 1:20 ratio. 50 µL of each standard and sample were mixed with 75 µL each of the manufacture's colour reagent A and B and incubated for 30 minutes at room temperature. All standards and samples were measured as duplicates. After the incubation, OD measurements were carried out at a wavelength of $\lambda = 450$ nm using a FLUOstar omega photometer (BMG Labtech GmbH, Ortenberg (Baden), Germany) and the accompanying software.

## 2.6 Statistical analysis

For statistical analysis and graphic representation Microsoft Excel 2016 for Windows 10 (Microsoft Corporation, Redmond, USA) and GraphPad Prism 8 (GraphPad Software, Inc., Boston, USA) were used. Briefly, normality was checked using Shapiro-Wilk test. Normally distributed variables were compared with Analysis of Variance (ANOVA) and non-parametric variables were using the Kruskal-Wallis test. Survival data of the mice were displayed in a Kaplan-Meier curve and tested for significant differences with the LogRank-test. A $p$-value $<0.05$ was considered statistically significant. Formal adjustment for multiple testing was not done.

# 3 Results

## 3.1 The DBA/2-mouse model

During the experiments, seven mice died prematurely or needed to be culled due to bad health condition:

- group 1 (vehicle-group (PBS)): n=3
- group 2 (reference antibody IDK-1): n=0
- group 3 (low-dose antibody FP21): n=1
- group 4 (medium-dose antibody FP21): n=1
- group 5 (high-dose antibody FP21): n=2

A LogRank-Test was used to test for potential significant differences. There were no significant differences between the five groups ($p$=0.5251). The overall survival after change of diet is shown in Figure 5

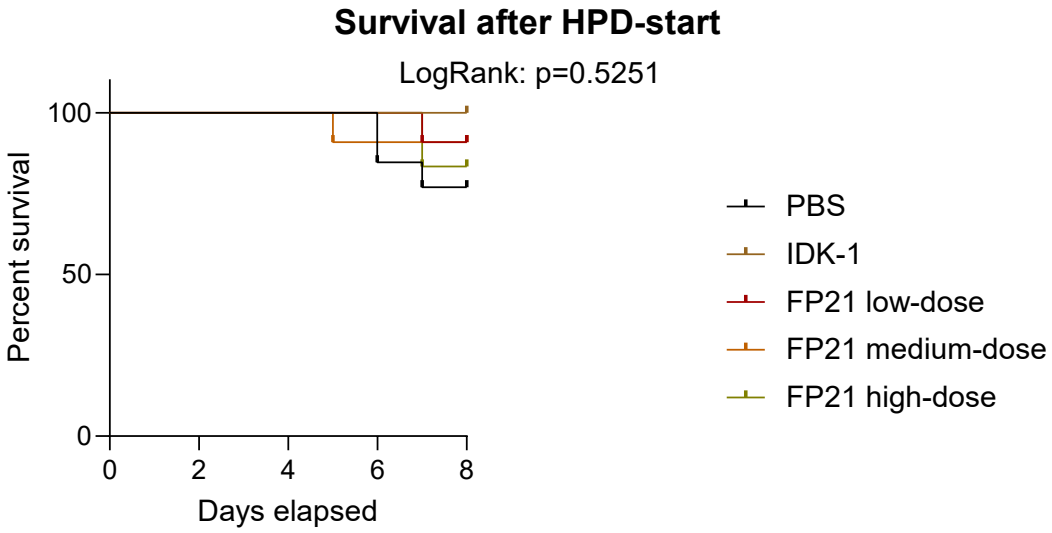


**Figure 5:** Kaplan–Meier curve after HPD-start

## 3.2 Calcium quantifications

### 3.2.1 Abdominal Aorta

The results of the median calcium concentrations of the abdominal aortas normalized to organ weight per group are displayed in Table 1:

**Table 1:** Median calcium concentrations and IQR of abdominal aortas normalized to organ weight

| Group | Antibody | Median calcium concentration [µg/mg] | *IQR* |
|---|---|---|---|
| 1 | PBS (vehicle-group) | 2.739 | 6.447 |
| 2 | IDK-1 (reference antibody) | 2.067 | 16.4126 |
| 3 | FP21 (low-dose) | 3.085 | 10.1122 |
| 4 | FP21 (medium-dose) | 9.240 | 8.801 |
| 5 | FP21 (high-dose) | 10.4 | 18.296 |

Kruskal-Wallis test revealed no significant differences between the five groups ($p$=0.3358).

Quantification of the median calcium concentrations normalized to protein content resulted in the data presented in Table 2:

**Table 2:** Median calcium concentrations and IQR of abdominal aortas normalized to protein content

| Group | Antibody | Median calcium concentration [µg/mg] | *IQR* |
|---|---|---|---|
| 1 | PBS (vehicle-group) | 69.15 | 215.6 |
| 2 | IDK-1 (reference antibody) | 46.55 | 656.61 |
| 3 | FP21 (low-dose) | 83.21 | 342.17 |
| 4 | FP21 (medium-dose) | 283.9 | 356.1 |
| 5 | FP21 (high-dose) | 510.8 | 686.1 |

Kruskal-Wallis test was used to detect potential significant differences. There were no significant differences between the five groups ($p$=0.2913).
Graphical representations of the results are shown in Figure 6.

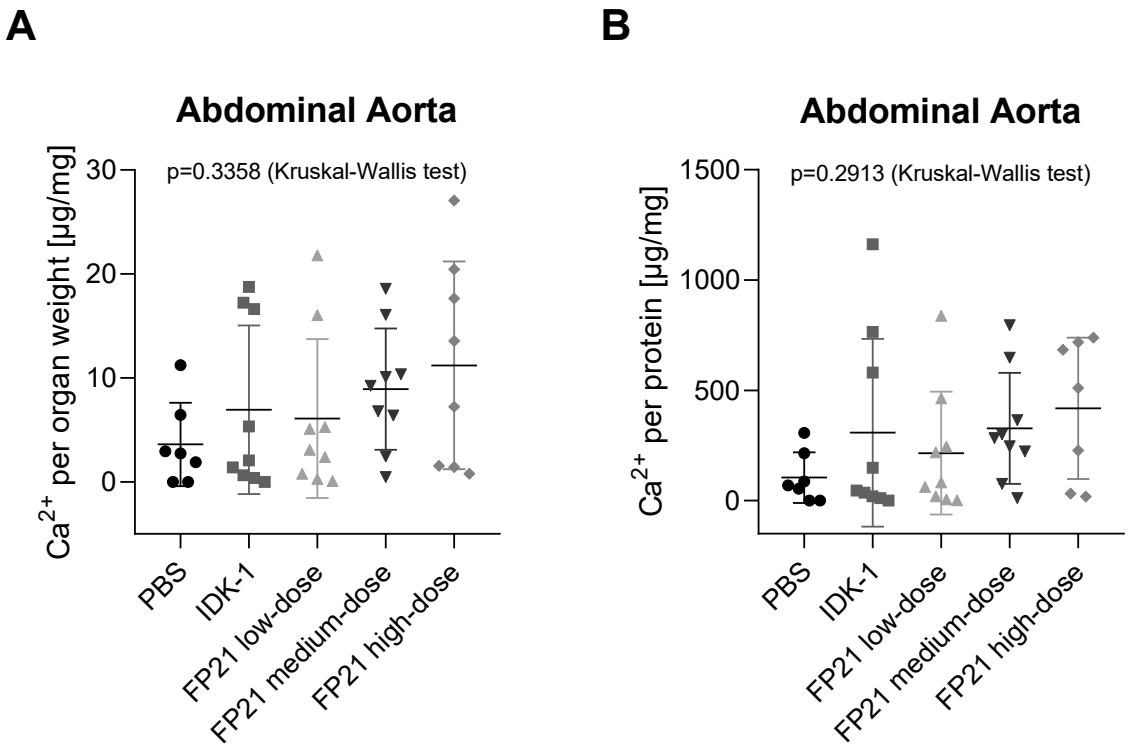


**Figure 6: A:** Calcium concentration of the abdominals aortas normalized to organ weight in different groups
**B:** Calcium concentration of the abdominals aortas normalized to protein content in different groups

### 3.2.2 Heart

The results of the mean calcium concentrations of the heart samples normalized to organ weight per group were as displayed in Table 3:

**Table 3:** Mean calcium concentrations and SD of heart samples normalized to organ weight.

| Group | Antibody | Mean calcium concentration [µg/mg] | *SD* |
|---|---|---|---|
| 1 | PBS (vehicle-group) | 12.36 | 6.348 |
| 2 | IDK-1 (reference antibody) | 10.34 | 5.937 |
| 3 | FP21 (low-dose) | 11.87 | 5.699 |
| 4 | FP21 (medium-dose) | 12.99 | 5.235 |
| 5 | FP21 (high-dose) | 9.514 | 6.003 |

ANOVA testing showed no significant differences between the five groups ($p$=0.7195).

Quantification of the mean calcium concentrations normalized to protein content resulted in the data presented in Table 4:

**Table 4:** Mean calcium concentrations and SD of heart samples normalized to protein content

| Group | Antibody | Mean calcium concentration [µg/mg] | *SD* |
|---|---|---|---|
| 1 | PBS (vehicle-group) | 140.3 | 78.57 |
| 2 | IDK-1 (reference antibody) | 115.5 | 69.03 |
| 3 | FP21 (low-dose) | 137.8 | 76.43 |
| 4 | FP21 (medium-dose) | 156.6 | 85.04 |
| 5 | FP21 (high-dose) | 97.76 | 61.35 |

There were no significant differences between the five groups using ANOVA ($p$=0.5243). Graphical representations of the results are shown in Figure 7.

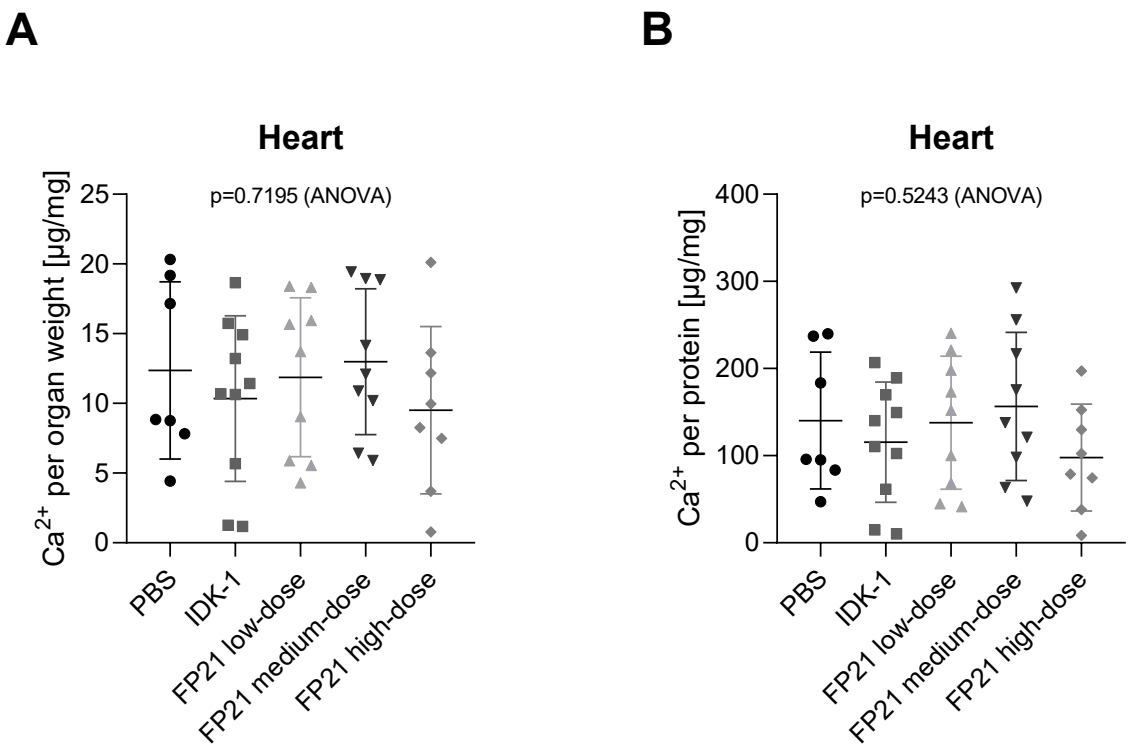


**Figure 7: A:** Calcium concentration of the heart samples normalized to organ weight in different groups
**B:** Calcium concentration of the heart samples normalized to protein content in different groups

### 3.2.3 Kidney

The results of the median calcium concentrations of the kidney samples normalized to organ weight per group were as displayed in Table 5:

**Table 5:** Median calcium concentrations and IQR of kidney samples normalized to organ weight

| Group | Antibody | Median calcium concentration [µg/mg] | *IQR* |
|---|---|---|---|
| 1 | PBS (vehicle-group) | 34.51 | 15.05 |
| 2 | IDK-1 (reference antibody) | 23.71 | 20.75 |
| 3 | FP21 (low-dose) | 28.06 | 14.52 |
| 4 | FP21 (medium-dose) | 24.73 | 19.23 |
| 5 | FP21 (high-dose) | 31.98 | 9.14 |

There were no significant differences between the five groups using Kruskal-Wallis test ($p$=0.2117).

Quantification of the mean calcium concentrations normalized to protein content resulted in the data presented in Table 6:

**Table 6:** Median calcium concentrations and IQR of kidney samples normalized to protein content

| Group | Antibody | Median calcium concentration [µg/mg] | *IQR* |
|---|---|---|---|
| 1 | PBS (vehicle-group) | 537.0 | 361.4 |
| 2 | IDK-1 (reference antibody) | 339.0 | 449.3 |
| 3 | FP21 (low-dose) | 441.6 | 193.3 |
| 4 | FP21 (medium-dose) | 336.8 | 339.8 |
| 5 | FP21 (high-dose) | 543.6 | 238.5 |

Kruskal-Wallis test was used to detect potential significant differences. There were no significant differences between the five groups ($p$=0.2501).
Graphical representations of the results are shown in Figure 8.

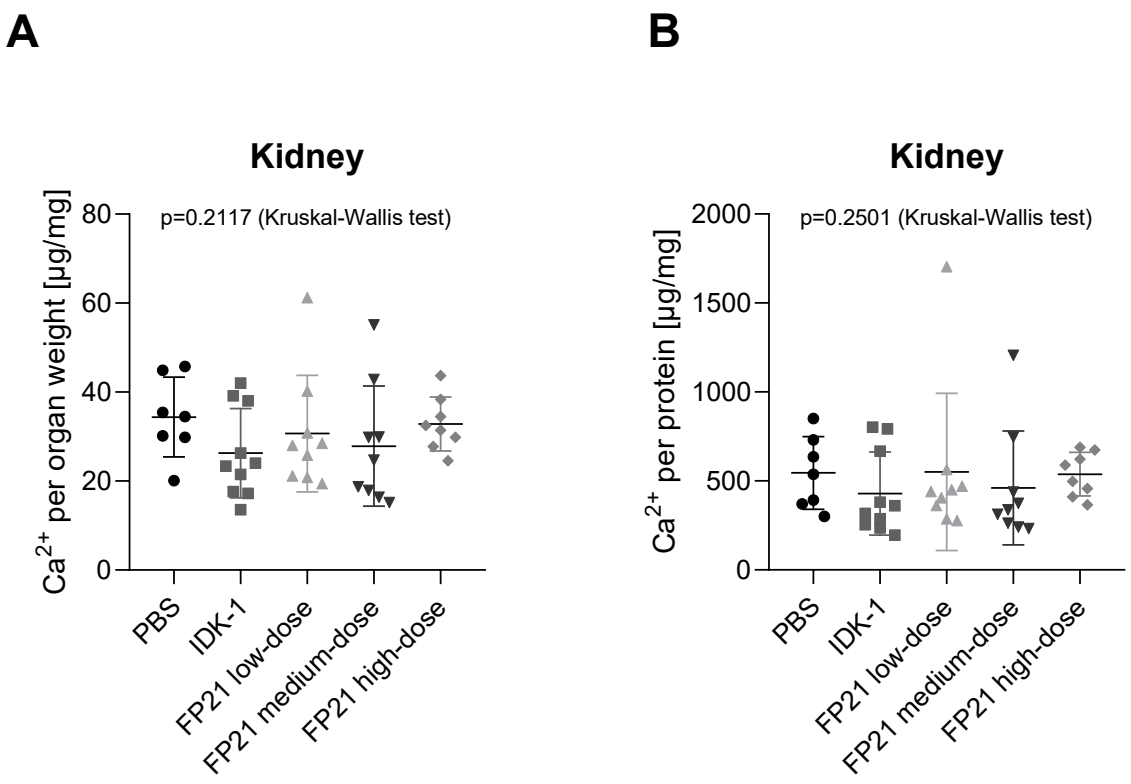


**Figure 8: A** Calcium concentration of the kidney samples normalized to organ weight in different groups **B:** Calcium concentration of the kidney samples normalized to protein content in different groups

## 3.3 Histological evaluation of calcium deposits

### 3.3.1 Heart

The mean percentages of the calcium deposits stained with Alizarin Red of the heart samples in different groups were as displayed in Table 7:

**Table 7:** Mean percentages and SD of Alizarin Red positive heart tissue

| Group | Antibody | Mean percentage of stained calcium deposits | *SD* |
|---|---|---|---|
| 1 | PBS (vehicle-group) | 13.14 | 4.692 |
| 2 | IDK-1 (reference antibody) | 10.88 | 6.137 |
| 3 | FP21 (low-dose) | 11.76 | 7.200 |
| 4 | FP21 (medium-dose) | 12.62 | 4.372 |
| 5 | FP21 (high-dose) | 9.814 | 5.653 |

ANOVA testing showed no significant differences between the five groups ($p$=0.7875). Exemplary slides with Alizarin Red positive heart tissues samples of all groups are shown in Figure 9 and in Figure 10A and B. A graphical representation of the results is shown in Figure 10C.

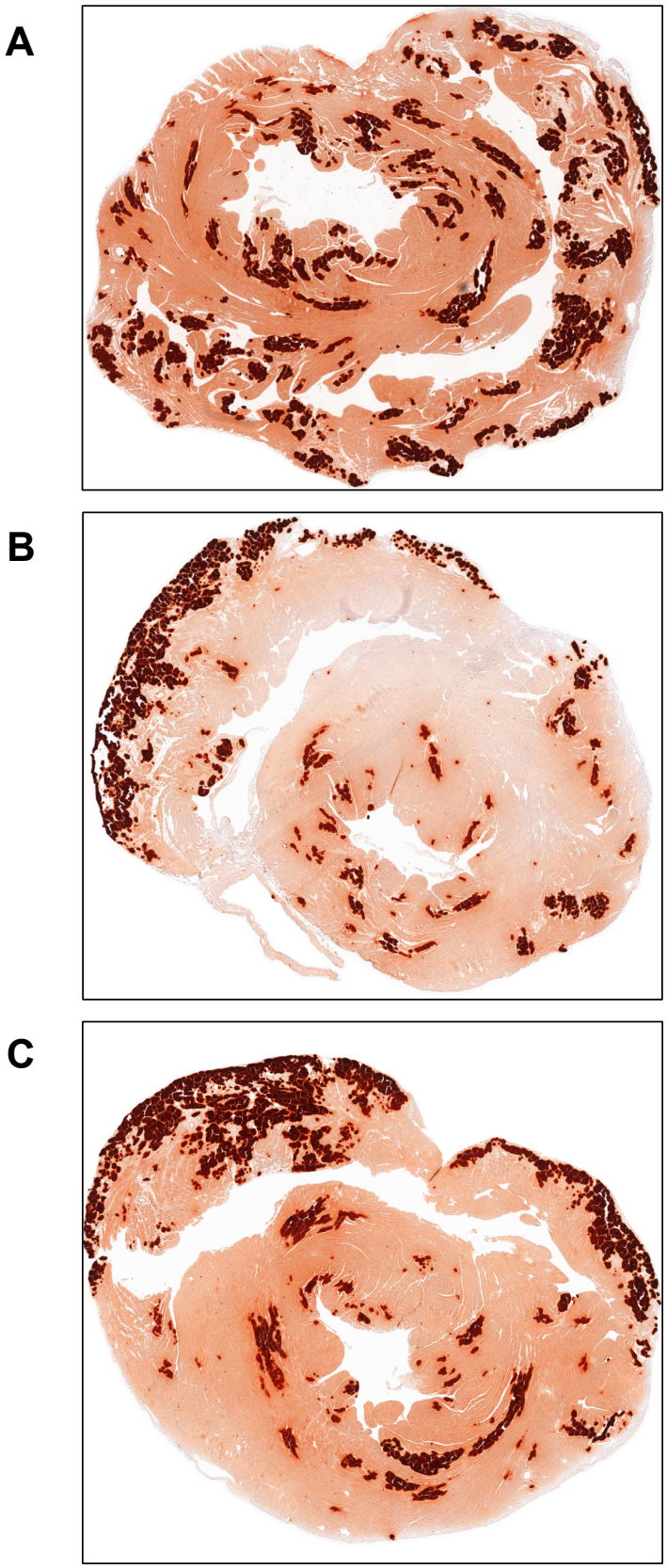


**Figure 9: A:** Heart sample stained with Alizarin Red (exemplary for group 1); 18.84 % stained areas (calcium deposits) **B:** Heart sample stained with Alizarin Red (exemplary for group 2); 9.76 % stained areas (calcium deposits) **C:** Heart sample stained with Alizarin Red (exemplary for group 3); 18.58 % stained areas (calcium deposits)

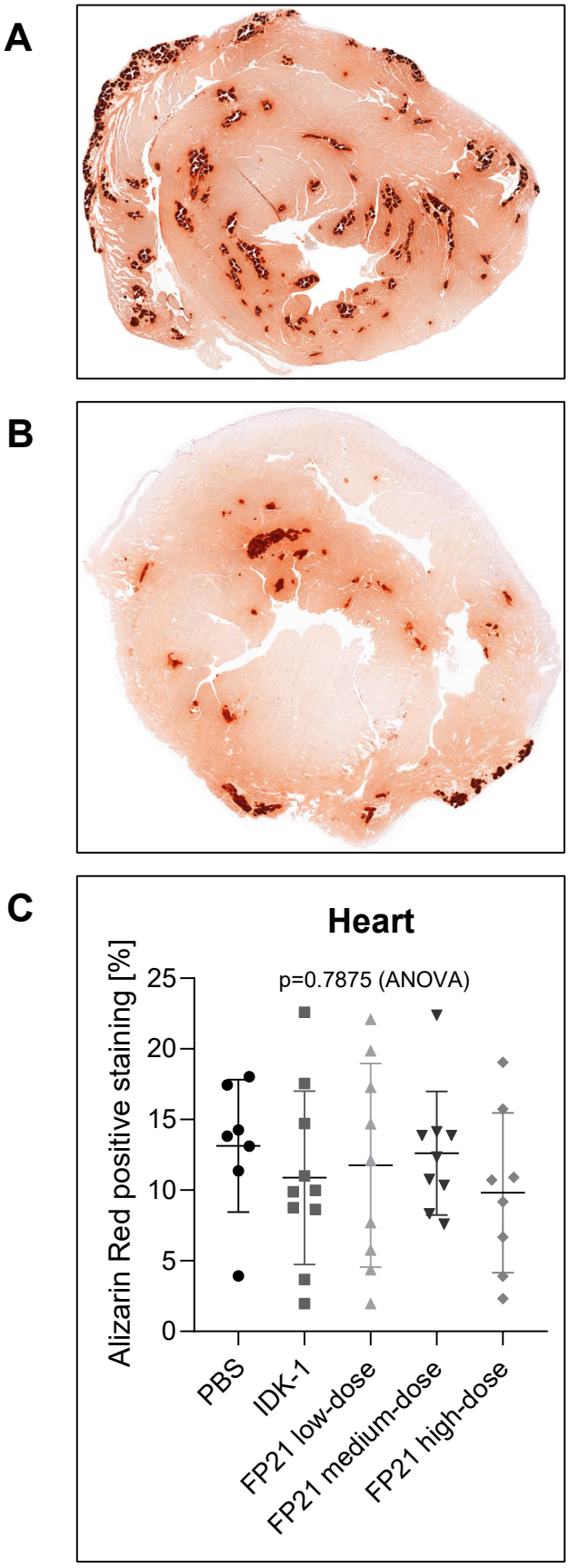


**Figure 10: A:** Heart sample stained with Alizarin Red (exemplary for group 4); 7.73 % stained areas (calcium deposits**) B:** Heart sample stained with Alizarin Red (exemplary for group 5); 2.36 % stained areas (calcium deposits) **C:** Percentage of Alizarin Red positive areas (calcium deposits) of each individual sample, grouped by the respective antibody group

### 3.3.2 Kidney

The median percentages of the calcium deposits stained with Alizarin Red of the kidney samples in different groups were as displayed in Table 8:

**Table 8:** Median percentages and IQR of Alizarin Red positive kidney tissue

| Group | Antibody | Median percentage of stained calcium deposits | *IQR* |
|---|---|---|---|
| 1 | PBS (vehicle-group) | 26.38 | 3.02 |
| 2 | IDK-1 (reference antibody) | 23.93 | 11.26 |
| 3 | FP21 (low-dose) | 20.98 | 7.98 |
| 4 | FP21 (medium-dose) | 20.67 | 8.83 |
| 5 | FP21 (high-dose) | 23.79 | 6.47 |

Kruskal-Wallis test was used to detect potential significant differences. There were no significant differences between the five groups ($p$=0.2441).

Exemplary slides with Alizarin Red positive kidney tissues samples of all are shown in Figure 11 and in Figure 12A and B. A graphical representation of the results is shown in Figure 12C.

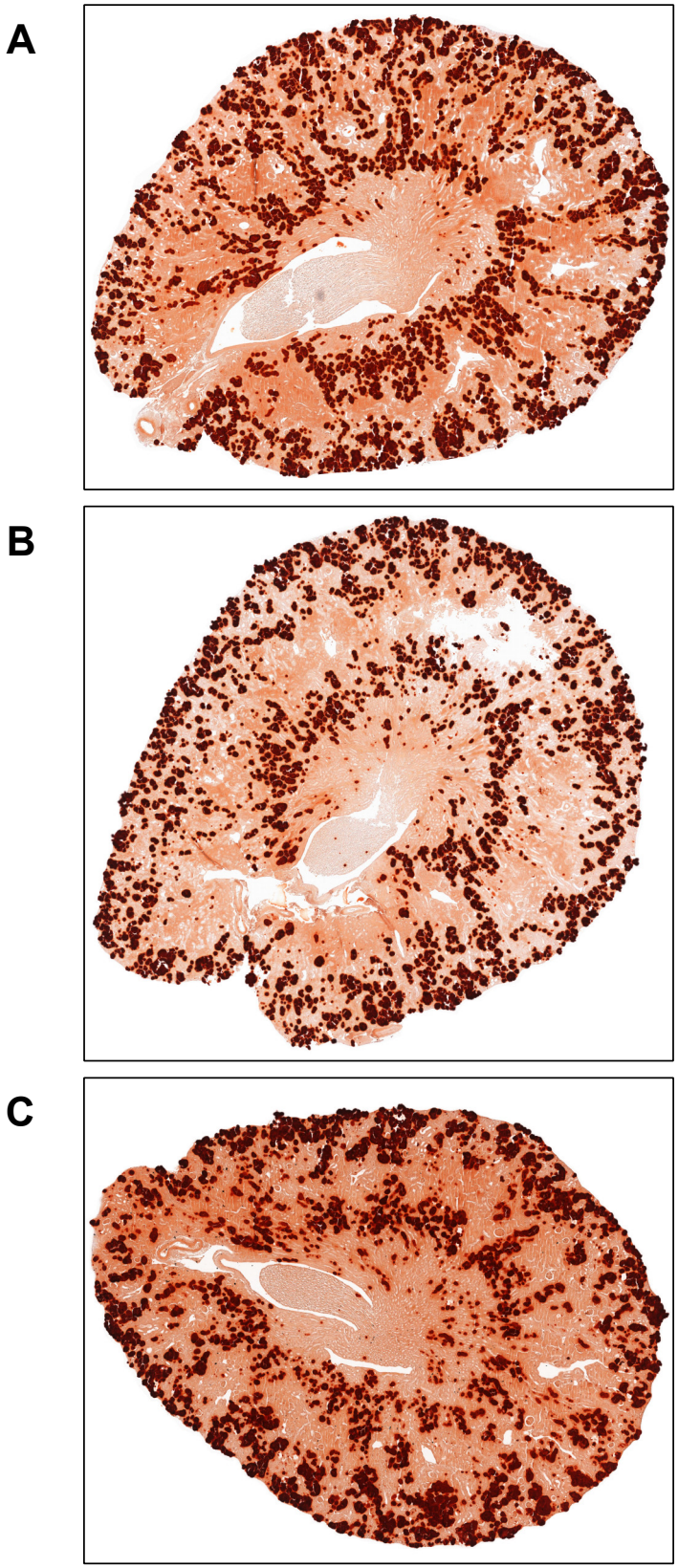


**Figure 11: A**: Kidney sample stained with Alizarin Red (exemplary for group 1); 27.30 % stained areas (calcium deposits) **B**: Kidney sample stained with Alizarin Red (exemplary for group 2); 32.13 % stained areas (calcium deposits) **C**: Kidney sample stained with Alizarin Red (exemplary for group 3); 30.86 % stained areas (calcium deposits)

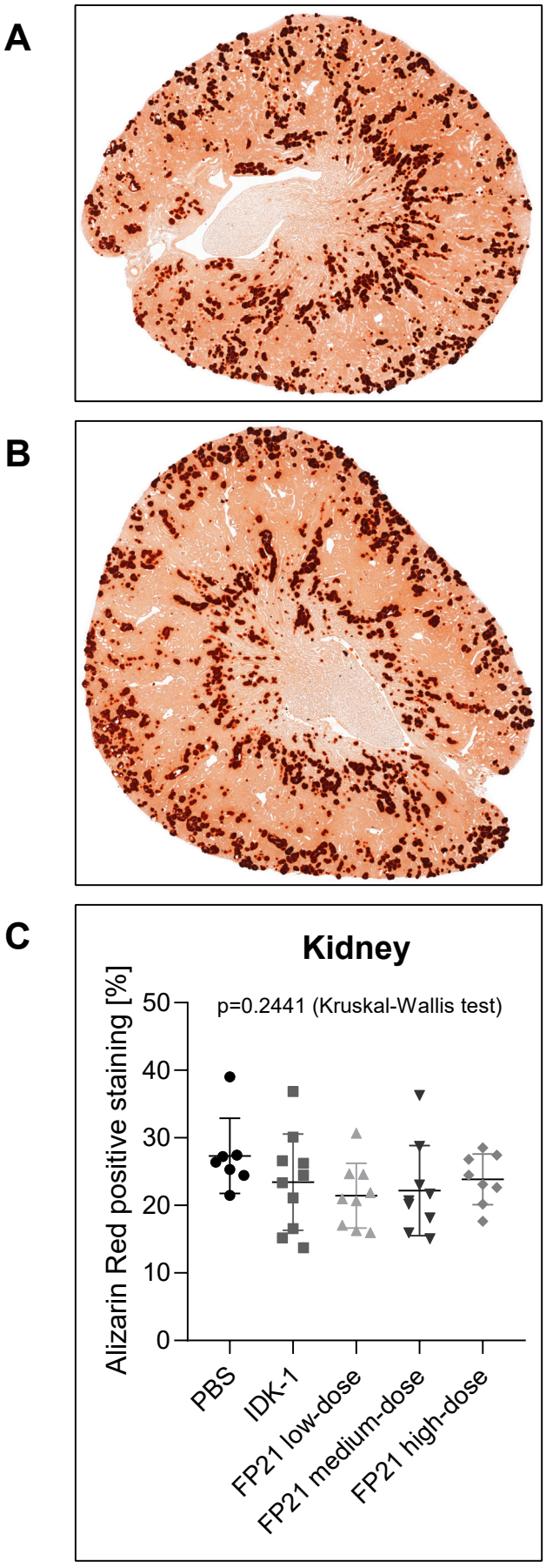


**Figure 12: A:** Kidney sample stained with Alizarin Red (exemplary for group 4); 15.34 % stained areas (calcium deposits**) B:** Kidney sample stained with Alizarin Red (exemplary for group 5); 22.74 % stained areas (calcium deposits) **C:** Percentage of Alizarin Red positive areas (calcium deposits) of each individual sample, grouped by the respective antibody group

## 3.4 Kidney function / BUN

BUN levels (as marker of kidney function) of the collected sera did not differ significantly between the different groups. The median levels in the five groups were as displayed in Table 9:

**Table 9:** Median concentrations and IQR of BUN measurements of the collected sera

| Group | Antibody | Median blood urea nitrogen concentration [mg/dL] | *IQR* |
|---|---|---|---|
| 1 | PBS (vehicle-group) | 87.13 | 44.42 |
| 2 | IDK-1 (reference antibody) | 76.86 | 8.39 |
| 3 | FP21 (low-dose) | 79.01 | 11.18 |
| 4 | FP21 (medium-dose) | 97.89 | 36.14 |
| 5 | FP21 (high-dose) | 88.09 | 27.87 |

Kruskal-Wallis test was used to detect potential differences. There were no significant differences between the five groups ($p$=0.1001).

A graphical representation is shown in Figure 13.

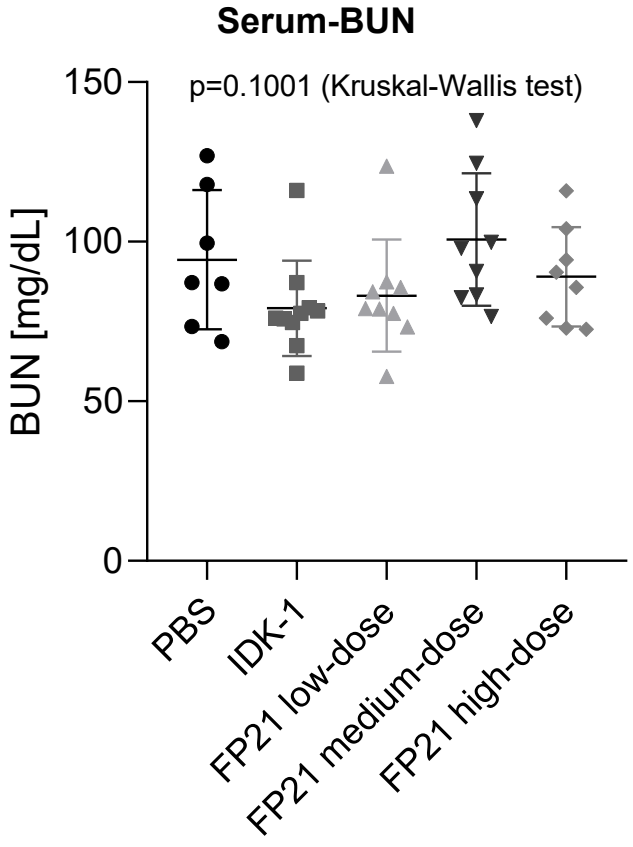


**Figure 13:** BUN levels in serum between different groups

## 3.5 Correlation between methods for calcium deposition assessment

To determine the extent of calcification of the heart and kidney samples, two different methods were used as described above. To further validate our results, we correlated results derived from calcium assay measurements and quantification of Alizarin Red-stained tissue. This resulted in a Pearson correlation coefficient (Pearson's r) of 0.6971 ($p$<0.0001) for the kidney samples. For the heart samples a Pearson's r of 0.8101 ($p$<0.0001) was calculated. Scatterplots as graphical representation of the correlation of the result are shown in Figure 14A for kidney samples and in Figure 14B for heart samples, respectively.

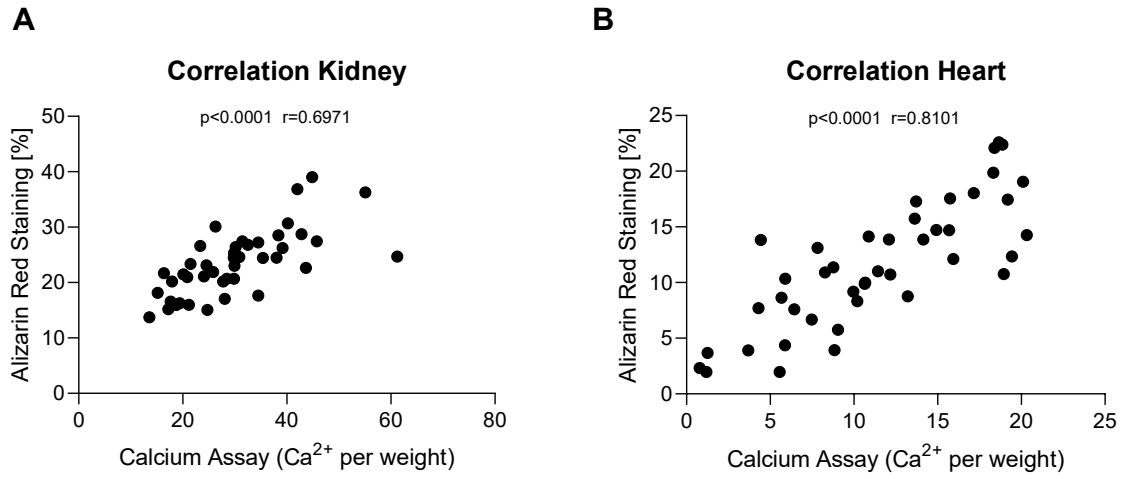


**Figure 14: A:** Scatterplot of corresponding results of calcium quantification and histological staining of each individual kidney sample **B:** Scatterplot of corresponding results of calcium quantification and histological staining of each individual heart sample)

# 4 Discussion

In the present study, we showed that calcification was not prevented by blocking BSP using the mouse monoclonal antibody FP21 in DBA/2 mice on a high phosphate diet as our results do not show any significant differences between the different antibody groups.

Not all mice survived the high-phosphate diet until the planned sacrifice at day 8. The highest number of deaths was in group 1 (PBS), followed by group 5 (high-dose FP21) with the second highest number of deaths. Deaths were not significantly different between the five groups, but they underline the severity of our mouse model. Furthermore, we did not aim to study a potential survival benefit, but to evaluate the effect of anti-BSP antibody treatment on organ calcium depositions. Our experience with DBA2/N mice has shown that there can be profound batch effects with regards to weight dynamics and robustness, which further complicates meaningful survival analysis.

Although we did not observe intergroup differences in calcification, we found severe calcification after only eight days of high-phosphate feeding. This is a relative short period of time regarding that other protocols of surgical and dietary models report time spans up to 8-12 weeks (126, 129). This underlines the high severity of our model. Active calcification is a result of mineralization in matrix vesicles, apoptotic bodies or secreted BSP. However, especially under extreme conditions, when calcium und phosphate concentrations surpass certain thresholds, there may be passive calcification, especially in *in vitro* models (159). Presently, we did not measure serum calcium or phosphate levels. But Kirsch et al. have shown that after 9 days of HPD, the Ca × P product may be as high as 19 $mmol^2/L^2$ in DBA/2 mice (160). Furthermore, depletion of regulatory T cells could influence the calcification propensity of the kidney, whereas heart calcification remained unchanged (160). In agreement with these findings, we report that the degree of calcification was more severe in the kidney than in the heart and the abdominal aorta showed the lowest calcium content. Thus, there may be tissue-dependent propensity for calcification with different pathways at play. Nevertheless, we could not find any difference in calcification between control and treatment with anti-BSP antibody in kidney, heart or abdominal aorta. Importantly, our findings were confirmed using two distinct methods of calcium quantification, i.e. staining of calcium deposits and colorimetric calcium measurements, which showed great intermethod agreement.

Alternatively, the antibody could be studied in a less severe DBA/2 model as shown by Frauscher et al. (140). Here, DBA/2 mice are kept on HPD for 4 to 7 days and then switched back to a standard chow diet for 84 days. This has been shown to mimic CKD-MBD including reduced kidney function, media calcification and bone abnormalities.

Kidney function was analysed by determination of BUN levels of all sacrificed mice. Our data did not show significant differences between the groups, consistently with similar calcium burden. Apart from BUN, other parameters can be used for determination of kidney function. Plasma creatinine and direct GFR measurement are to be noted here. We only used BUN, as plasma creatinine levels have limited informative value. This is due to mice physiology as, firstly, they are nocturnal animals and hence have a different circadian rhythm (161).
Secondly, mice do secret creatinine actively to a significant degree (up to 50 %). Therefore, serum creatinine levels stay low despite of impaired kidney function (162).
Furthermore, estimation of kidney function via serum creatinine is erroneous in der presence of cachectic weight loss (like in our mice) (163). The gold standard to evaluate kidney function is direct GFR measurement by means of inulin clearance. However, direct GFR measurement, e.g. by transcutaneous measurement of marker clearance, is laborious and stressful for mice. Finally, our study was not designed to assess for minute differences in kidney function, so we measured BUN levels as a crude estimate. Additionally, discrepancies in kidney function are highly unlikely due to the comparable extent of kidney calcification (and thus comparable kidney damage) between all groups.

There are certain limitations to our study.
First, our study may have been limited by the group size. We observed a broad distribution of individual data points, which reflects the interindividual and interbatch differences in DBA2/N mice. Larger group sizes may have allowed us to overcome this limitation. However, we did not observe a trend in our data, which would hint towards a problem with power. Furthermore, previous studies with this model have found treatment effects using similar group sizes (50, 136, 160).
Second, the antibody treatment duration may have been too short. To remedy this limitation, a time course experiment could be performed comparing varying exposure times to the anti-BSP antibody prior to HPD.

Another limitation is, that the used calcification model is rather severe. This can be seen in the high mortality of up to 30 % in the control group (group 1). It is tempting to speculate that anti-BSP antibody could be protective in a model with longer duration and more gradual calcification. However, other treatments like inhibition of the mechanistic Target of Rapamycin (mTOR) have had a beneficial effect in our model, which even translated in a survival benefit (136).

Moreover, we did not assess for tissue anti-BSP antibody binding. It is conceivable that anti-BSP antibody may not have bound to endogenous BSP or that antibodies against the anti-BSP antibody – similar to anti-drug antibodies – have formed. To mitigate this limitation, one could perform immunohistochemical workup of the tissues to stain for BSP and/or FP21. Furthermore, mice sera could be checked for the presence of FP21-antibodies as well as BSP serum levels.

Finally, our study does not allow us to differentiate between active or passive calcification. With the latter, any intervention that is not aimed at lowering the calcium phosphate product or designed to interfere with the physicochemical process of calcification including anti-BSP antibodies would be *a priori* futile. The osteoblastic transdifferentiation of VSMCs is a hallmark of vascular calcification and precedes the deposition of calcium phosphate crystal (97). In order to be able to determine the causative process of calcification in our model, an extensive experimental setup would be necessary. Clarification would necessitate laborious time course experiments, in which the presence of calcification and of osteoblastic transdifferentiation markers would be evaluated during HPD. Upregulation or increased expression of osteogenic markers, such as Runx2 or MSX-9 and loss of SM22α or smooth muscle α-actin could be examined using real-time / quantitative polymerase chain reaction (qPCR), western blot or immunohistochemical staining. In theory, a switch of VSCMs from a contractile to an osteoblastic/chondrogenic phenotype preceding calcification would indicate an active process, whereas simultaneous calcification and phenotypic switch or delayed phenotypic switch would be indicative of a passive process.

# References


1. Group IGOCW. KDIGO 2012 clinical practice guideline for the evaluation and management of chronic kidney disease. Kidney Int Suppl. 2013;3(Supl. 1):1-150.
2. Brandes R, Lang F, Schmidt RF. Physiologie des Menschen: mit Pathophysiologie. 32. Auflage ed. Brandes R, Lang F, Schmidt RF, editors. Berlin: Springer; 2019.
3. Waas T, Schulz A, Lotz J, Rossmann H, Pfeiffer N, Beutel ME, et al. Distribution of estimated glomerular filtration rate and determinants of its age dependent loss in a German population-based study. Sci Rep. 2021;11(1):10165.
4. Levey AS, Stevens LA, Schmid CH, Zhang YL, Castro AF, 3rd, Feldman HI, et al. A new equation to estimate glomerular filtration rate. Ann Intern Med. 2009;150(9):604-12.
5. Braun J, Müller-Wieland D, Altiok E, Krautzig S. Basislehrbuch Innere Medizin. 7. Auflage ed: München : Elsevier; 2022. XXIV, 1184 Seiten, Illustrationen, Diagramme p.
6. Herold G. Innere Medizin 2023. Berlin, Boston: De Gruyter; 2023.
7. Kidney Disease: Improving Global Outcomes Blood Pressure Work G. KDIGO 2021 Clinical Practice Guideline for the Management of Blood Pressure in Chronic Kidney Disease. Kidney Int. 2021;99(3S):S1-S87.
8. Meyer TW, Hostetter TH. Uremia. N Engl J Med. 2007;357(13):1316-25.
9. Clase CM, Carrero J-J, Ellison DH, Grams ME, Hemmelgarn BR, Jardine MJ, et al. Potassium homeostasis and management of dyskalemia in kidney diseases: conclusions from a Kidney Disease: Improving Global Outcomes (KDIGO) Controversies Conference. Kidney International. 2020;97(1):42-61.
10. Maxwell PH, Eckardt K-U. HIF prolyl hydroxylase inhibitors for the treatment of renal anaemia and beyond. Nature Reviews Nephrology. 2016;12(3):157-68.
11. Chen N, Hao C, Peng X, Lin H, Yin A, Hao L, et al. Roxadustat for Anemia in Patients with Kidney Disease Not Receiving Dialysis. New England Journal of Medicine. 2019;381(11):1001-10.
12. Cheung AK, Chang TI, Cushman WC, Furth SL, Hou FF, Ix JH, et al. Executive summary of the KDIGO 2021 Clinical Practice Guideline for the Management of Blood Pressure in Chronic Kidney Disease. Kidney Int. 2021;99(3):559-69.
13. Schmitt R. [Inhibition of the renin-angiotensin-aldosterone system]. Nephrologe. 2022;17(1):26-33.

14. Perkovic V, Jardine MJ, Neal B, Bompoint S, Heerspink HJL, Charytan DM, et al. Canagliflozin and Renal Outcomes in Type 2 Diabetes and Nephropathy. N Engl J Med. 2019;380(24):2295-306.
15. Heerspink HJL, Stefansson BV, Correa-Rotter R, Chertow GM, Greene T, Hou FF, et al. Dapagliflozin in Patients with Chronic Kidney Disease. N Engl J Med. 2020;383(15):1436-46.
16. Dumann E, Menne J. [SGLT2 inhibitors: What is new?]. Nephrologe. 2021;16(4):241-55.
17. Höfler G, Kreipe HH, Moch HU-, -Fischer-Verlag. Pathologie. 6., vollständig überarbeitete Auflage ed. München: Elsevier, Urban & Fischer; 2019. XXVII, 1071 Seiten p.
18. Lüllmann-Rauch R, Asan E. Taschenlehrbuch Histologie. 6., vollständig überarbeitete Auflage ed. Stuttgart ; New York: Georg Thieme Verlag; 2019.
19. Hartmann M, Pabst M-A, Dohr G. Zytologie, Histologie und mikroskopische Anatomie : licht- und elektronenmikroskopischer Bildatlas. 5., überarbeitete Auflage ed: Wien : facultas.wuv; 2011. p. 1 Online-Ressource (139 Seiten), Illustrationen.
20. Kelvinsong. Artery (https://commons.wikimedia.org/wiki/File:Artery.svg) licensed under CC BY-SA 3.0 Deed (https://creativecommons.org/licenses/by-sa/3.0/deed.en).
21. Herrington W, Lacey B, Sherliker P, Armitage J, Lewington S. Epidemiology of Atherosclerosis and the Potential to Reduce the Global Burden of Atherothrombotic Disease. Circ Res. 2016;118(4):535-46.
22. Timmis A, Vardas P, Townsend N, Torbica A, Katus H, De Smedt D, et al. European Society of Cardiology: cardiovascular disease statistics 2021. European Heart Journal. 2022;43(8):716-99.
23. Shi X, Gao J, Lv Q, Cai H, Wang F, Ye R, et al. Calcification in Atherosclerotic Plaque Vulnerability: Friend or Foe? Front Physiol. 2020;11:56.
24. Libby P, Buring JE, Badimon L, Hansson GK, Deanfield J, Bittencourt MS, et al. Atherosclerosis. Nat Rev Dis Primers. 2019;5(1):56.
25. Visseren FLJ, Mach F, Smulders YM, Carballo D, Koskinas KC, Back M, et al. 2021 ESC Guidelines on cardiovascular disease prevention in clinical practice. Eur Heart J. 2021;42(34):3227-337.
26. Kidney Disease: Improving Global Outcomes Blood Pressure Work G. KDIGO Clinical Practice Guidline for Lipid Managemnt in Chronic Kidney Disease. Kidney Int Suppl. 2013;3:259-305.

27. Gavornik P, Galbavy S. Clinical picture of arteriolosclerosis. Bratisl Lek Listy. 2001;102(7):326-31.
28. Damjanov I. Chapter 7 - The Blood Vessels. In: Damjanov I, editor. Pathology Secrets (Third Edition). Philadelphia: Mosby; 2009. p. 121-36.
29. Dos Santos VP, Pozzan G, Castelli V, Caffaro RA. Arteriosclerosis, atherosclerosis, arteriolosclerosis, and Monckeberg medial calcific sclerosis: what is the difference? J Vasc Bras. 2021;20:e20200211.
30. Villa-Bellosta R, Egido J. Phosphate, pyrophosphate, and vascular calcification: a question of balance. Eur Heart J. 2017;38(23):1801-4.
31. Lanzer P, Hannan FM, Lanzer JD, Janzen J, Raggi P, Furniss D, et al. Medial Arterial Calcification: JACC State-of-the-Art Review. J Am Coll Cardiol. 2021;78(11):1145-65.
32. Wu M, Rementer C, Giachelli CM. Vascular calcification: an update on mechanisms and challenges in treatment. Calcif Tissue Int. 2013;93(4):365-73.
33. Lanzer P, Boehm M, Sorribas V, Thiriet M, Janzen J, Zeller T, et al. Medial vascular calcification revisited: review and perspectives. European Heart Journal. 2014;35(23):1515-25.
34. Mönckeberg JG. Über die reine Mediaverkalkung der Extremitätenarterien und ihr Verhalten zur Arteriosklerose. Virchows Archiv für pathologische Anatomie und Physiologie und für klinische Medizin. 1903;171(1):141-67.
35. London GM. Arterial calcification: cardiovascular function and clinical outcome. Nefrologia. 2011;31(6):644-7.
36. Hoek AG, Zwakenberg SR, Elders PJM, de Jong PA, Spiering W, Bartstra JW, et al. An elevated ankle-brachial index is not a valid proxy for peripheral medial arterial calcification. Atherosclerosis. 2021;323:13-9.
37. Kamenskiy A, Poulson W, Sim S, Reilly A, Luo J, MacTaggart J. Prevalence of Calcification in Human Femoropopliteal Arteries and its Association with Demographics, Risk Factors, and Arterial Stiffness. Arterioscler Thromb Vasc Biol. 2018;38(4):e48-e57.
38. Kaess BM, Rong J, Larson MG, Hamburg NM, Vita JA, Levy D, et al. Aortic stiffness, blood pressure progression, and incident hypertension. JAMA. 2012;308(9):875-81.
39. Chirinos JA, Segers P. Noninvasive evaluation of left ventricular afterload: part 2: arterial pressure-flow and pressure-volume relations in humans. Hypertension. 2010;56(4):563-70.

40. Chirinos JA, Segers P, Hughes T, Townsend R. Large-Artery Stiffness in Health and Disease: JACC State-of-the-Art Review. J Am Coll Cardiol. 2019;74(9):1237-63.
41. Byrom FB. The hypertensive vascular crisis: an experimental study: Butterworth-Heinemann London; 2013.
42. O'Rourke MF, Safar ME. Relationship between aortic stiffening and microvascular disease in brain and kidney: cause and logic of therapy. Hypertension. 2005;46(1):200-4.
43. O'Neill WC, Han KH, Schneider TM, Hennigar RA. Prevalence of nonatheromatous lesions in peripheral arterial disease. Arterioscler Thromb Vasc Biol. 2015;35(2):439-47.
44. Majesky MW. Developmental basis of vascular smooth muscle diversity. Arterioscler Thromb Vasc Biol. 2007;27(6):1248-58.
45. Kirby ML, Gale TF, Stewart DE. Neural crest cells contribute to normal aorticopulmonary septation. Science. 1983;220(4601):1059-61.
46. Vrancken Peeters M-PFM, Gittenberger-de Groot AC, Mentink MMT, Poelmann RE. Smooth muscle cells and fibroblasts of the coronary arteries derive from epithelial-mesenchymal transformation of the epicardium. Anatomy and Embryology. 1999;199(4):367-78.
47. Owens GK. Regulation of differentiation of vascular smooth muscle cells. Physiol Rev. 1995;75(3):487-517.
48. Rzucidlo EM, Martin KA, Powell RJ. Regulation of vascular smooth muscle cell differentiation. J Vasc Surg. 2007;45 Suppl A:A25-32.
49. Owens GK, Kumar MS, Wamhoff BR. Molecular Regulation of Vascular Smooth Muscle Cell Differentiation in Development and Disease. Physiological Reviews. 2004;84(3):767-801.
50. Kirsch AH, Kirsch A, Artinger K, Schabhuttl C, Goessler W, Klymiuk I, et al. Heterogeneous susceptibility for uraemic media calcification and concomitant inflammation within the arterial tree. Nephrol Dial Transplant. 2015;30(12):1995-2005.
51. Hao H, Gabbiani G, Bochaton-Piallat ML. Arterial smooth muscle cell heterogeneity: implications for atherosclerosis and restenosis development. Arterioscler Thromb Vasc Biol. 2003;23(9):1510-20.
52. Ahmed S, Warren DT. Vascular smooth muscle cell contractile function and mechanotransduction. Vessel Plus. 2018;2:36.
53. Feil S, Hofmann F, Feil R. SM22alpha modulates vascular smooth muscle cell phenotype during atherogenesis. Circ Res. 2004;94(7):863-5.

54. Tyson KL, Reynolds JL, McNair R, Zhang Q, Weissberg PL, Shanahan CM. Osteo/chondrocytic transcription factors and their target genes exhibit distinct patterns of expression in human arterial calcification. Arterioscler Thromb Vasc Biol. 2003;23(3):489-94.
55. Montezano AC, Zimmerman D, Yusuf H, Burger D, Chignalia AZ, Wadhera V, et al. Vascular smooth muscle cell differentiation to an osteogenic phenotype involves TRPM7 modulation by magnesium. Hypertension. 2010;56(3):453-62.
56. Schlieper G, Schurgers L, Brandenburg V, Reutelingsperger C, Floege J. Vascular calcification in chronic kidney disease: an update. Nephrol Dial Transplant. 2016;31(1):31-9.
57. Steitz SA, Speer MY, Curinga G, Yang HY, Haynes P, Aebersold R, et al. Smooth muscle cell phenotypic transition associated with calcification: upregulation of Cbfa1 and downregulation of smooth muscle lineage markers. Circ Res. 2001;89(12):1147-54.
58. Durham AL, Speer MY, Scatena M, Giachelli CM, Shanahan CM. Role of smooth muscle cells in vascular calcification: implications in atherosclerosis and arterial stiffness. Cardiovasc Res. 2018;114(4):590-600.
59. Kang YH, Jin JS, Yi DW, Son SM. Bone morphogenetic protein-7 inhibits vascular calcification induced by high vitamin D in mice. Tohoku J Exp Med. 2010;221(4):299-307.
60. Cancela ML, Laize V, Conceicao N, Kempf H, Murshed M. Keutel Syndrome, a Review of 50 Years of Literature. Front Cell Dev Biol. 2021;9:642136.
61. Kapustin AN, Davies JD, Reynolds JL, McNair R, Jones GT, Sidibe A, et al. Calcium regulates key components of vascular smooth muscle cell-derived matrix vesicles to enhance mineralization. Circ Res. 2011;109(1):e1-12.
62. Poterucha TJ, Goldhaber SZ. Warfarin and Vascular Calcification. Am J Med. 2016;129(6):635 e1-4.
63. Szweras M, Liu D, Partridge EA, Pawling J, Sukhu B, Clokie C, et al. alpha 2-HS glycoprotein/fetuin, a transforming growth factor-beta/bone morphogenetic protein antagonist, regulates postnatal bone growth and remodeling. J Biol Chem. 2002;277(22):19991-7.
64. Demetriou M, Binkert C, Sukhu B, Tenenbaum HC, Dennis JW. Fetuin/alpha2-HS glycoprotein is a transforming growth factor-beta type II receptor mimic and cytokine antagonist. J Biol Chem. 1996;271(22):12755-61.

65. Uitto J, Li Q, Jiang Q. Pseudoxanthoma elasticum: molecular genetics and putative pathomechanisms. J Invest Dermatol. 2010;130(3):661-70.
66. Kauffenstein G, Pizard A, Le Corre Y, Vessieres E, Grimaud L, Toutain B, et al. Disseminated arterial calcification and enhanced myogenic response are associated with abcc6 deficiency in a mouse model of pseudoxanthoma elasticum. Arterioscler Thromb Vasc Biol. 2014;34(5):1045-56.
67. Fleisch H, Russell RG, Straumann F. Effect of pyrophosphate on hydroxyapatite and its implications in calcium homeostasis. Nature. 1966;212(5065):901-3.
68. Lomashvili KA, Cobbs S, Hennigar RA, Hardcastle KI, O'Neill WC. Phosphate-induced vascular calcification: role of pyrophosphate and osteopontin. J Am Soc Nephrol. 2004;15(6):1392-401.
69. Jackson EK, Cheng D, Verrier JD, Janesko-Feldman K, Kochanek PM. Interactive roles of CD73 and tissue nonspecific alkaline phosphatase in the renal vascular metabolism of 5'-AMP. Am J Physiol Renal Physiol. 2014;307(6):F680-5.
70. Jin H, St Hilaire C, Huang Y, Yang D, Dmitrieva NI, Negro A, et al. Increased activity of TNAP compensates for reduced adenosine production and promotes ectopic calcification in the genetic disease ACDC. Sci Signal. 2016;9(458):ra121.
71. Picher M, Burch LH, Hirsh AJ, Spychala J, Boucher RC. Ecto 5'-nucleotidase and nonspecific alkaline phosphatase. Two AMP-hydrolyzing ectoenzymes with distinct roles in human airways. J Biol Chem. 2003;278(15):13468-79.
72. Roberts S, Narisawa S, Harmey D, Millán JL, Farquharson C. Functional Involvement of PHOSPHO1 in Matrix Vesicle–Mediated Skeletal Mineralization. Journal of Bone and Mineral Research. 2007;22(4):617-27.
73. Kiffer-Moreira T, Yadav MC, Zhu D, Narisawa S, Sheen C, Stec B, et al. Pharmacological inhibition of PHOSPHO1 suppresses vascular smooth muscle cell calcification. J Bone Miner Res. 2013;28(1):81-91.
74. Nakano-Kurimoto R, Ikeda K, Uraoka M, Nakagawa Y, Yutaka K, Koide M, et al. Replicative senescence of vascular smooth muscle cells enhances the calcification through initiating the osteoblastic transition. Am J Physiol Heart Circ Physiol. 2009;297(5):H1673-84.
75. Hu MC, Shi M, Zhang J, Quinones H, Griffith C, Kuro-o M, et al. Klotho deficiency causes vascular calcification in chronic kidney disease. J Am Soc Nephrol. 2011;22(1):124-36.

76. Kuro-o M, Matsumura Y, Aizawa H, Kawaguchi H, Suga T, Utsugi T, et al. Mutation of the mouse klotho gene leads to a syndrome resembling ageing. Nature. 1997;390(6655):45-51.
77. Byon CH, Javed A, Dai Q, Kappes JC, Clemens TL, Darley-Usmar VM, et al. Oxidative stress induces vascular calcification through modulation of the osteogenic transcription factor Runx2 by AKT signaling. J Biol Chem. 2008;283(22):15319-27.
78. Alam MU, Kirton JP, Wilkinson FL, Towers E, Sinha S, Rouhi M, et al. Calcification is associated with loss of functional calcium-sensing receptor in vascular smooth muscle cells. Cardiovasc Res. 2009;81(2):260-8.
79. Lin ME, Chen T, Leaf EM, Speer MY, Giachelli CM. Runx2 Expression in Smooth Muscle Cells Is Required for Arterial Medial Calcification in Mice. Am J Pathol. 2015;185(7):1958-69.
80. Mary A, Hénaut L, Boudot C, Six I, Brazier M, Massy ZA, et al. Calcitriol Prevents In Vitro Vascular Smooth Muscle Cell Mineralization by Regulating Calcium-Sensing Receptor Expression. Endocrinology. 2015;156(6):1965-74.
81. Bas A, Lopez I, Perez J, Rodriguez M, Aguilera-Tejero E. Reversibility of calcitriol-induced medial artery calcification in rats with intact renal function. J Bone Miner Res. 2006;21(3):484-90.
82. Shroff R, Egerton M, Bridel M, Shah V, Donald AE, Cole TJ, et al. A bimodal association of vitamin D levels and vascular disease in children on dialysis. J Am Soc Nephrol. 2008;19(6):1239-46.
83. Leopold JA. MicroRNAs Regulate Vascular Medial Calcification. Cells. 2014;3(4):963-80.
84. Li X, Giachelli CM. Sodium-dependent phosphate cotransporters and vascular calcification. Curr Opin Nephrol Hypertens. 2007;16(4):325-8.
85. Li X, Yang HY, Giachelli CM. BMP-2 promotes phosphate uptake, phenotypic modulation, and calcification of human vascular smooth muscle cells. Atherosclerosis. 2008;199(2):271-7.
86. Zhou W, Simic P, Zhou IY, Caravan P, Vela Parada X, Wen D, et al. Kidney glycolysis serves as a mammalian phosphate sensor that maintains phosphate homeostasis. J Clin Invest. 2023;133(8).
87. Yoshida T, Yamashita M, Horimai C, Hayashi M. Smooth Muscle-Selective Nuclear Factor-kappaB Inhibition Reduces Phosphate-Induced Arterial Medial Calcification in Mice With Chronic Kidney Disease. J Am Heart Assoc. 2017;6(11).

88. Zhang D, Bi X, Liu Y, Huang Y, Xiong J, Xu X, et al. High Phosphate-Induced Calcification of Vascular Smooth Muscle Cells is Associated with the TLR4/NF-kappab Signaling Pathway. Kidney Blood Press Res. 2017;42(6):1205-15.
89. Lee HL, Woo KM, Ryoo HM, Baek JH. Tumor necrosis factor-alpha increases alkaline phosphatase expression in vascular smooth muscle cells via MSX2 induction. Biochem Biophys Res Commun. 2010;391(1):1087-92.
90. Raaz U, Schellinger IN, Chernogubova E, Warnecke C, Kayama Y, Penov K, et al. Transcription Factor Runx2 Promotes Aortic Fibrosis and Stiffness in Type 2 Diabetes Mellitus. Circ Res. 2015;117(6):513-24.
91. Voelkl J, Luong TT, Tuffaha R, Musculus K, Auer T, Lian X, et al. SGK1 induces vascular smooth muscle cell calcification through NF-kappaB signaling. J Clin Invest. 2018;128(7):3024-40.
92. Cai T, Sun D, Duan Y, Wen P, Dai C, Yang J, et al. WNT/beta-catenin signaling promotes VSMCs to osteogenic transdifferentiation and calcification through directly modulating Runx2 gene expression. Exp Cell Res. 2016;345(2):206-17.
93. Yao L, Sun YT, Sun W, Xu TH, Ren C, Fan X, et al. High phosphorus level leads to aortic calcification via beta-catenin in chronic kidney disease. Am J Nephrol. 2015;41(1):28-36.
94. Shao JS, Cheng SL, Pingsterhaus JM, Charlton-Kachigian N, Loewy AP, Towler DA. Msx2 promotes cardiovascular calcification by activating paracrine Wnt signals. J Clin Invest. 2005;115(5):1210-20.
95. Willert J, Epping M, Pollack JR, Brown PO, Nusse R. A transcriptional response to Wnt protein in human embryonic carcinoma cells. BMC Dev Biol. 2002;2:8.
96. Yamada S, Tokumoto M, Tatsumoto N, Taniguchi M, Noguchi H, Nakano T, et al. Phosphate overload directly induces systemic inflammation and malnutrition as well as vascular calcification in uremia. Am J Physiol Renal Physiol. 2014;306(12):F1418-28.
97. Voelkl J, Lang F, Eckardt KU, Amann K, Kuro OM, Pasch A, et al. Signaling pathways involved in vascular smooth muscle cell calcification during hyperphosphatemia. Cell Mol Life Sci. 2019;76(11):2077-91.
98. Agharazii M, St-Louis R, Gautier-Bastien A, Ung RV, Mokas S, Lariviere R, et al. Inflammatory cytokines and reactive oxygen species as mediators of chronic kidney disease-related vascular calcification. Am J Hypertens. 2015;28(6):746-55.

99. Sun M, Chang Q, Xin M, Wang Q, Li H, Qian J. Endogenous bone morphogenetic protein 2 plays a role in vascular smooth muscle cell calcification induced by interleukin 6 in vitro. Int J Immunopathol Pharmacol. 2017;30(3):227-37.
100. Alesutan I, Musculus K, Castor T, Alzoubi K, Voelkl J, Lang F. Inhibition of Phosphate-Induced Vascular Smooth Muscle Cell Osteo-/Chondrogenic Signaling and Calcification by Bafilomycin A1 and Methylamine. Kidney Blood Press Res. 2015;40(5):490-9.
101. Hiyama A, Gogate SS, Gajghate S, Mochida J, Shapiro IM, Risbud MV. BMP-2 and TGF-β stimulate expression of β1,3-glucuronosyl transferase 1 (GlcAT-1) in nucleus pulposus cells through AP1, TonEBP, and Sp1: Role of MAPKs. Journal of Bone and Mineral Research. 2010;25(5):1179-90.
102. Caron MM, van der Windt AE, Emans PJ, van Rhijn LW, Jahr H, Welting TJ. Osmolarity determines the in vitro chondrogenic differentiation capacity of progenitor cells via nuclear factor of activated T-cells 5. Bone. 2013;53(1):94-102.
103. Zhao MM, Xu MJ, Cai Y, Zhao G, Guan Y, Kong W, et al. Mitochondrial reactive oxygen species promote p65 nuclear translocation mediating high-phosphate-induced vascular calcification in vitro and in vivo. Kidney Int. 2011;79(10):1071-9.
104. Reynolds JL, Joannides AJ, Skepper JN, McNair R, Schurgers LJ, Proudfoot D, et al. Human vascular smooth muscle cells undergo vesicle-mediated calcification in response to changes in extracellular calcium and phosphate concentrations: a potential mechanism for accelerated vascular calcification in ESRD. J Am Soc Nephrol. 2004;15(11):2857-67.
105. Proudfoot D, Skepper JN, Hegyi L, Bennett MR, Shanahan CM, Weissberg PL. Apoptosis regulates human vascular calcification in vitro: evidence for initiation of vascular calcification by apoptotic bodies. Circ Res. 2000;87(11):1055-62.
106. Shroff R, Long DA, Shanahan C. Mechanistic insights into vascular calcification in CKD. J Am Soc Nephrol. 2013;24(2):179-89.
107. Hunter GK, Goldberg HA. Nucleation of hydroxyapatite by bone sialoprotein. Proc Natl Acad Sci U S A. 1993;90(18):8562-5.
108. Mills KT, Xu Y, Zhang W, Bundy JD, Chen CS, Kelly TN, et al. A systematic analysis of worldwide population-based data on the global burden of chronic kidney disease in 2010. Kidney Int. 2015;88(5):950-7.

109. Benz K, Varga I, Neureiter D, Campean V, Daniel C, Heim C, et al. Vascular inflammation and media calcification are already present in early stages of chronic kidney disease. Cardiovasc Pathol. 2017;27:57-67.
110. Voelkl J. Welche Rolle spielen Phosphathaushalt und Gefäßverkalkungen bei der chronischen Niereninsuffizienz? Der Nephrologe. 2019;14(6):475-8.
111. Moorthi RN, Moe SM. CKD-mineral and bone disorder: core curriculum 2011. Am J Kidney Dis. 2011;58(6):1022-36.
112. Li J, Molnar MZ, Zaritsky JJ, Sim JJ, Streja E, Kovesdy CP, et al. Correlates of parathyroid hormone concentration in hemodialysis patients. Nephrol Dial Transplant. 2013;28(6):1516-25.
113. Lomashvili KA, Khawandi W, O'Neill WC. Reduced plasma pyrophosphate levels in hemodialysis patients. J Am Soc Nephrol. 2005;16(8):2495-500.
114. Zou D, Wu W, He Y, Ma S, Gao J. The role of klotho in chronic kidney disease. BMC Nephrol. 2018;19(1):285.
115. Urakawa I, Yamazaki Y, Shimada T, Iijima K, Hasegawa H, Okawa K, et al. Klotho converts canonical FGF receptor into a specific receptor for FGF23. Nature. 2006;444(7120):770-4.
116. Moe SM. Klotho: a master regulator of cardiovascular disease? Circulation. 2012;125(18):2181-3.
117. Hene RJ, Boer P, Koomans HA, Mees EJ. Plasma aldosterone concentrations in chronic renal disease. Kidney Int. 1982;21(1):98-101.
118. Voelkl J, Alesutan I, Leibrock CB, Quintanilla-Martinez L, Kuhn V, Feger M, et al. Spironolactone ameliorates PIT1-dependent vascular osteoinduction in klotho-hypomorphic mice. J Clin Invest. 2013;123(2):812-22.
119. Moe SM, Duan D, Doehle BP, O'Neill KD, Chen NX. Uremia induces the osteoblast differentiation factor Cbfa1 in human blood vessels. Kidney Int. 2003;63(3):1003-11.
120. Chiang CK, Hsu SP, Pai MF, Peng YS, Ho TI, Liu SH, et al. Plasma Interleukin-18 Levels in Chronic Renal Failure and Continuous Ambulatory Peritoneal Dialysis. Blood Purification. 2005;23(2):144-8.
121. Zhang K, Zhang Y, Feng W, Chen R, Chen J, Touyz RM, et al. Interleukin-18 Enhances Vascular Calcification and Osteogenic Differentiation of Vascular Smooth Muscle Cells Through TRPM7 Activation. Arterioscler Thromb Vasc Biol. 2017;37(10):1933-43.

122. Schelski N, Luong TTD, Lang F, Pieske B, Voelkl J, Alesutan I. SGK1-dependent stimulation of vascular smooth muscle cell osteo-/chondrogenic transdifferentiation by interleukin-18. Pflugers Arch. 2019;471(6):889-99.
123. Herrmann J, Babic M, Tolle M, van der Giet M, Schuchardt M. Research Models for Studying Vascular Calcification. Int J Mol Sci. 2020;21(6).
124. Kaspareit-Rittinghausen J, Rapp K, Deerberg F, Wcislo A, Messow C. Hereditary Polycystic Kidney Disease Associated with Osteorenal Syndrome in Rats. Veterinary Pathology. 1989;26(3):195-201.
125. Ng K, Hildreth CM, Phillips JK, Avolio AP. Aortic stiffness is associated with vascular calcification and remodeling in a chronic kidney disease rat model. Am J Physiol Renal Physiol. 2011;300(6):F1431-6.
126. Gagnon RF, Duguid WP. A reproducible model for chronic renal failure in the mouse. Urol Res. 1983;11(1):11-4.
127. CHANUTIN A, FERRIS EB, Jr. EXPERIMENTAL RENAL INSUFFICIENCY PRODUCED BY PARTIAL NEPHRECTOMY: I. CONTROL DIET. Archives of Internal Medicine. 1932;49(5):767-87.
128. Yokozawa T, Oura H, Okada T. Metabolic effects of dietary purine in rats. J Nutr Sci Vitaminol (Tokyo). 1982;28(5):519-26.
129. Shobeiri N, Pang J, Adams MA, Holden RM. Cardiovascular disease in an adenine-induced model of chronic kidney disease: the temporal link between vascular calcification and haemodynamic consequences. Journal of Hypertension. 2013;31(1).
130. El-Abbadi MM, Pai AS, Leaf EM, Yang HY, Bartley BA, Quan KK, et al. Phosphate feeding induces arterial medial calcification in uremic mice: role of serum phosphorus, fibroblast growth factor-23, and osteopontin. Kidney Int. 2009;75(12):1297-307.
131. Luo G, Ducy P, McKee MD, Pinero GJ, Loyer E, Behringer RR, et al. Spontaneous calcification of arteries and cartilage in mice lacking matrix GLA protein. Nature. 1997;386(6620):78-81.
132. Schäfer C, Heiss A, Schwarz A, Westenfeld R, Ketteler M, Floege J, et al. The serum protein α2–Heremans-Schmid glycoprotein/fetuin-A is a systemically acting inhibitor of ectopic calcification. The Journal of Clinical Investigation. 2003;112(3):357-66.

133. Razzaque MS, Sitara D, Taguchi T, St-Arnaud R, Lanske B. Premature aging-like phenotype in fibroblast growth factor 23 null mice is a vitamin D-mediated process. FASEB J. 2006;20(6):720-2.
134. Ivandic BT, Utz HF, Kaczmarek PM, Aherrahrou Z, Axtner SB, Klepsch C, et al. New Dyscalc loci for myocardial cell necrosis and calcification (dystrophic cardiac calcinosis) in mice. Physiol Genomics. 2001;6(3):137-44.
135. Eaton GJ, Custer RP, Johnson FN, Stabenow KT. Dystrophic cardiac calcinosis in mice: genetic, hormonal, and dietary influences. Am J Pathol. 1978;90(1):173-86.
136. Frauscher B, Kirsch AH, Schabhuttl C, Schweighofer K, Ketszeri M, Pollheimer M, et al. Autophagy Protects From Uremic Vascular Media Calcification. Front Immunol. 2018;9:1866.
137. Meng H, Vera I, Che N, Wang X, Wang SS, Ingram-Drake L, et al. Identification of Abcc6 as the major causal gene for dystrophic cardiac calcification in mice through integrative genomics. Proc Natl Acad Sci U S A. 2007;104(11):4530-5.
138. Berndt A, Li Q, Potter CS, Liang Y, Silva KA, Kennedy V, et al. A single-nucleotide polymorphism in the Abcc6 gene associates with connective tissue mineralization in mice similar to targeted models for pseudoxanthoma elasticum. J Invest Dermatol. 2013;133(3):833-6.
139. Jansen RS, Kucukosmanoglu A, de Haas M, Sapthu S, Otero JA, Hegman IE, et al. ABCC6 prevents ectopic mineralization seen in pseudoxanthoma elasticum by inducing cellular nucleotide release. Proc Natl Acad Sci U S A. 2013;110(50):20206-11.
140. Frauscher B, Artinger K, Kirsch AH, Aringer I, Moschovaki-Filippidou F, Ketszeri M, et al. A New Murine Model of Chronic Kidney Disease-Mineral and Bone Disorder. Int J Endocrinol. 2017;2017:1659071.
141. Fisher LW, Torchia DA, Fohr B, Young MF, Fedarko NS. Flexible structures of SIBLING proteins, bone sialoprotein, and osteopontin. Biochem Biophys Res Commun. 2001;280(2):460-5.
142. Ganss B, Kim RH, Sodek J. Bone sialoprotein. Crit Rev Oral Biol Med. 1999;10(1):79-98.
143. Zaia J, Boynton R, Heinegard D, Barry F. Posttranslational modifications to human bone sialoprotein determined by mass spectrometry. Biochemistry. 2001;40(43):12983-91.
144. Wuttke M, Muller S, Nitsche DP, Paulsson M, Hanisch FG, Maurer P. Structural characterization of human recombinant and bone-derived bone sialoprotein. Functional

implications for cell attachment and hydroxyapatite binding. J Biol Chem. 2001;276(39):36839-48.
145. Vincent K, Durrant MC. A structural and functional model for human bone sialoprotein. J Mol Graph Model. 2013;39:108-17.
146. Goldberg HA, Warner KJ, Stillman MJ, Hunter GK. Determination of the hydroxyapatite-nucleating region of bone sialoprotein. Connect Tissue Res. 1996;35(1-4):385-92.
147. Oldberg A, Franzen A, Heinegard D. The primary structure of a cell-binding bone sialoprotein. J Biol Chem. 1988;263(36):19430-2.
148. Ruoslahti E. RGD and other recognition sequences for integrins. Annu Rev Cell Dev Biol. 1996;12:697-715.
149. Marcus durrant. Molecular model of human bone sialoprotein (https://commons.wikimedia.org/wiki/File:Bone_Sialoprotein_Model.png) licensed under CC BY-SA 4.0 Deed (https://creativecommons.org/licenses/by-sa/4.0/deed.en)
150. Chen JK, Shapiro HS, Wrana JL, Reimers S, Heersche JN, Sodek J. Localization of bone sialoprotein (BSP) expression to sites of mineralized tissue formation in fetal rat tissues by in situ hybridization. Matrix. 1991;11(2):133-43.
151. Bellahcene A, Merville MP, Castronovo V. Expression of bone sialoprotein, a bone matrix protein, in human breast cancer. Cancer Res. 1994;54(11):2823-6.
152. Bellahcene A, Menard S, Bufalino R, Moreau L, Castronovo V. Expression of bone sialoprotein in primary human breast cancer is associated with poor survival. Int J Cancer. 1996;69(4):350-3.
153. Bellahcène A, Van Riet I, De Greef C, Antoine N, Young MF, Van Camp B, et al. Bone sialoprotein mRNA and protein expression in human multiple myeloma cell lines and patients. British Journal of Haematology. 2000;111(4):1118-21.
154. Bellahcene A, Albert V, Pollina L, Basolo F, Fisher LW, Castronovo V. Ectopic expression of bone sialoprotein in human thyroid cancer. Thyroid. 1998;8(8):637-41.
155. Waltregny D, Bellahcene A, Van Riet I, Fisher LW, Young M, Fernandez P, et al. Prognostic value of bone sialoprotein expression in clinically localized human prostate cancer. J Natl Cancer Inst. 1998;90(13):1000-8.
156. Karadag A, Ogbureke KU, Fedarko NS, Fisher LW. Bone sialoprotein, matrix metalloproteinase 2, and alpha(v)beta3 integrin in osteotropic cancer cell invasion. J Natl Cancer Inst. 2004;96(12):956-65.

157. Zepp M, Kovacheva M, Altankhuyag M, Westphal G, Berger I, Gather KS, et al. IDK1 is a rat monoclonal antibody against hypoglycosylated bone sialoprotein with application as biomarker and therapeutic agent in breast cancer skeletal metastasis. The Journal of Pathology: Clinical Research. 2018;4(1):55-68.
158. Bankhead P, Loughrey MB, Fernández JA, Dombrowski Y, McArt DG, Dunne PD, et al. QuPath: Open source software for digital pathology image analysis. Scientific Reports. 2017;7(1):16878.
159. Villa-Bellosta R, Millan A, Sorribas V. Role of calcium-phosphate deposition in vascular smooth muscle cell calcification. Am J Physiol Cell Physiol. 2011;300(1):C210-20.
160. Kirsch AH, Smaczny N, Riegelbauer V, Sedej S, Hofmeister A, Stojakovic T, et al. Regulatory T cells improve nephrocalcinosis but not dystrophic cardiac calcinosis in DBA/2 mice. Am J Pathol. 2013;183(2):382-90.
161. Meneton P, Ichikawa I, Inagami T, Schnermann J. Renal physiology of the mouse. Am J Physiol Renal Physiol. 2000;278(3):F339-51.
162. Eisner C, Faulhaber-Walter R, Wang Y, Leelahavanichkul A, Yuen PS, Mizel D, et al. Major contribution of tubular secretion to creatinine clearance in mice. Kidney Int. 2010;77(6):519-26.
163. Nankivell BJ, Nankivell LFJ, Elder GJ, Gruenewald SM. How unmeasured muscle mass affects estimated GFR and diagnostic inaccuracy. EClinicalMedicine. 2020;29-30:100662.